UNIVERSIDADE ESTADUAL DE CAMPINAS
Faculdade de Engenharia Elétrica e de Computação

Aparna Aravind Payyazhi

Recursive Blind Phase Search Architecture for Phase Recovery at High Error Rates

Arquitetura Recursiva de Busca de Fase Cega para Recuperação de Fase em Altas Taxas de Erro

Campinas

2019

UNIVERSIDADE ESTADUAL DE CAMPINAS
Faculdade de Engenharia Elétrica e de Computação

Aparna Aravind Payyazhi

Recursive Blind Phase Search Architecture for Phase Recovery at High Error Rates

Arquitetura Recursiva de Busca de Fase Cega para Recuperação de Fase em Altas Taxas de Erro

Dissertation presented to the School of Electrical and Computer Engineering of the University of Campinas as a requirement for the Master's Degree in Electrical Engineering, in the area of Telecommunications and Telematics.

Dissertação apresentada à Faculdade de Engenharia Elétrica e de Computação da Universidade Estadual de Campinas como requisito para a obtenção do título de Mestra em Engenharia Elétrica, na Área de Telecomunicações e Telemática.

Supervisor: Prof. Dr. Darli Augusto de Arruda Mello

Este exemplar corresponde à versão final da tese defendida pelo aluno Aparna Aravind Payyazhi, e orientada pelo Prof. Dr. Darli Augusto de Arruda Mello

Campinas

2019

Agência(s) de fomento e nº(s) de processo(s): CNPq, 166631/2017-5

Ficha catalográfica
Universidade Estadual de Campinas
Biblioteca da Área de Engenharia e Arquitetura
Elizangela Aparecida dos Santos Souza - CRB 8/8098

P297r

Payyazhi, Aparna Aravind, 1992-
Recursive blind phase search architecture for phase recovery at high error rates / Aparna Aravind Payyazhi. – Campinas, SP : [s.n.], 2019.

Orientador: Darli Augusto de Arruda Mello.
Dissertação (mestrado) – Universidade Estadual de Campinas, Faculdade de Engenharia Elétrica e de Computação.

1. Comunicações ópticas. 2. Processamento digital de sinais. I. Mello, Darli Augusto de Arruda, 1976-. II. Universidade Estadual de Campinas. Faculdade de Engenharia Elétrica e de Computação. III. Título.

Informações para Biblioteca Digital

Título em outro idioma: Arquitetura recursiva de busca de fase cega para recuperação de fase em altas taxas de erro
Palavras-chave em inglês:
Optical communications
Digital signal processing
Área de concentração: Telecomunicações e Telemática
Titulação: Mestra em Engenharia Elétrica
Banca examinadora:
Darli Augusto de Arruda Mello [Orientador]
Karcius Day Rosário Assis
Yuzo Iano
Data de defesa: 16-01-2019
Programa de Pós-Graduação: Engenharia Elétrica

COMMISÃO JULGADORA – DISSERTAÇÃO DE MESTRADO

Candidato: Aparna Aravind Payyazhi RA:190744

Data da Defesa: 16 de janeiro de 2019

Título da Tese: "Recursive Blind Phase Search Architecture for Phase Recovery at High Error Rates (Arquitetura Recursiva de Busca de Fase Cega para Recuperação de Fase em Altas Taxas de Erro)".

Prof. Dr. Darli Augusto de Arruda Mello (Presidente, FEEC/UNICAMP)

Prof. Dr. Karcius Day Rosário Assis (UFBA)

Prof. Dr. Yuzo Iano (FEEC/UNICAMP)

A ata de defesa, com as respectivas assinaturas dos membros da Comissão Julgadora, encontra-se no SIGA (Sistema de Fluxo de Dissertação/Tese) e na Secretaria de Pós-Graduação da Faculdade de Engenharia Elétrica e de Computação.

To my husband Ajay Mohan
To my parents Parukutty and Aravindan
To my sister Anupama

Acknowledgements

Initially, I would like to thank god for blessing me to do my Post Graduation. I express my gratitude to my parents who loved, cared and prayed for me. Also, I would like to thank my husband, without his encouragement and support I would not have pursued my dream. I am deeply grateful to my advisor Prof. Dr. Darli Augusto de Arruda Mello for giving me the opportunity to pursue my masters, for his guidance, help, and support during this journey. I thank Prof. Dalton Soares for his encouragement. I would like to express my gratitude to André Luiz Nunes de Souza for supporting me. I also thank my colleagues; whose unconditional help and support increased my confidence in my work. Finally, I want to thank the University of Campinas and CNPq for giving me the best platform and financial support.

Depois de parar de aprender, você começa a morrer.

Albert Einstein

Abstract

The demand of advanced developments in the field of optical communication systems is increasing day by day, and large amounts of data need to be transmitted. In this context, high-order modulation formats support the transmission of large data volumes with high spectral efficiency. However, because of the smaller Euclidean distance between the constellation points, these modulation formats are more susceptible to the phase noise generated by the transmitter and local oscillator lasers. This leads to stringent requirements of carrier phase recovery algorithms. In modern coherent optical communications systems, the blind phase search (BPS) algorithm emerged as a widely accepted solution for the phase recovery of square quadrature amplitude modulation (QAM) constellations. However, at low signal to noise ratios, it requires very long noise-rejection filters, whose length can reach hundreds of symbols. In this thesis, we propose a phase recovery architecture suitable for channels with low phase noise and high additive noise. The algorithm replaces window filters of the BPS algorithm by forgetting factors. The proposed forgetting-factor BPS (FF-BPS) algorithm is evaluated using 16-QAM and 64-QAM constellations through simulation and experiments. Its performance is also compared to that of a decision directed (DD) implementation. Simulations and experimental results indicate that the proposed algorithm achieves equivalent performance as unilateral BPS (using current and past symbols) and better performance than the DD algorithm. However, its performance is still surpassed by that obtained by the bilateral BPS algorithm (using current, past and future symbols).

Keywords: optical communications; phase noise; digital signal processing; blind phase search algorithm; forgetting factor algorithm; decision-directed algorithm.

Resumo

A demanda por desenvolvimentos avançados no campo de sistemas de comunicação óptica está aumentando dia a dia, e grandes quantidades de dados precisam ser transmitidas. Neste contexto, os formatos de modulação de alta ordem suportam a transmissão de grandes volumes de dados com alta eficiência espectral. No entanto, devido à menor distância Euclidiana entre os pontos da constelação, esses formatos de modulação são mais suscetíveis ao ruído de fase gerado pelos lasers do transmissor e do oscilador local. Isso leva a requisitos rigorosos de algoritmos de recuperação de fase da portadora. Em sistemas modernos de comunicações ópticas coerentes, o algoritmo de busca de fase cega (blind phase search - BPS) surgiu como uma solução amplamente aceita para a recuperação de fase de constelações quadradas de modulação de amplitude em quadratura (quadrature amplitude modulation - QAM). No entanto, a baixas taxas de relação sinal ruído requerem filtros de rejeição de ruído para o BPS muito longos, cujo comprimento pode alcançar centenas de símbolos. Nesta tese, propomos uma arquitetura de recuperação de fase adequada para canais com baixo ruído de fase e alto ruído aditivo. O algoritmo substitui os filtros de janelamento do algoritmo BPS por fatores de esquecimento. O algoritmo proposto (forgetting-factor BPS - FF-BPS) é avaliado usando constelações 16-QAM e 64-QAM por meio de simulação e experimentos. Seu desempenho também é comparado ao de uma implementação direcionada por decisão (DD). Simulações e resultados experimentais indicam que o algoritmo proposto alcança desempenho equivalente ao BPS unilateral (usando símbolos atuais e passados) e melhor desempenho que o algoritmo DD. No entanto, seu desempenho ainda é superado pelo obtido por meio do algoritmo BPS bilateral (usando símbolos atuais, passados e futuros).

Palavras-chaves: comunicações óptica; ruído de fase; processamento digital de sinais; algoritmo de busca de fase cega; algoritmo de fator de esquecimento; algoritmo dirigido por decisão.

List of Figures

List of Tables

Acronyms

ADC - Analog to digital converter.

AM - Amplitude modulation.

ASE - Amplified spontaneous emission.

ASK - Amplitude-shift keying.

AWGN - Additive white Gaussian noise.

BER - Bit error rate.

BPS - Blind phase search.

CD - Chromatic dispersion.

CMA - Constant modulus algorithm.

DD - Decision directed.

DGD - Differential group delay.

DSP - Digital signal processing.

ECL - External cavity laser.

FF-BPS - Forgetting factor BPS.

FFT - Fast Fourier transform.

FIR - Finite impulse response.

FSK - Frequency shift keying.

GVD - Group velocity dispersion parameter.

IF - Intermediate frequency.

IQ - In-phase and quadrature modulator.

LED - Light emitting diode.

MIMO - Multiple-input multiple output.

MZM - Mach-Zehnder modulator.

OSA - Optical spectrum analyzer.

OSNR - optical signal to noise ratio.

PAM - Pulse Amplitude Modulation.

PDF - Probability density function.

PDM - Polarization division multiplexing.

PM - Phase modulator.

PU - Phase unwrapper.

QAM - Quadrature amplitude modulation.

QM - Quadrature modulator.

QPSK - quadrature phase-shift keying.

RDE - Radially directed equalizer.

SNR - Signal to noise ratio.

WDM - Wavelength division multiplexing.

Symbols

$\Delta\nu$ - Sum of receiver and transmitter laser linewidths.

T_s - Symbol periods.

$E_{out}(t)$ - Output electric field.

$E_{in}(t)$ - Input electric field.

$\phi(t)$ - Phase shift.

$u(t)$ - Driving voltage.

V_π - Voltage required to achieve phase shift.

P - Average optical power.

Z - Propagation distance.

α - Attenuation constant.

L - Fiber length.

r - Received signal.

s - Transmitted signal.

w - AWGN noise.

h - Planck's constant.

f_c - Photon frequency.

n_{sp} - Spontaneous emission factor.

G - Amplifier gain.

B_0 - Optical bandwidth.

P_N - ASE noise power.

N_1 - Atomic population in the ground state.

N_2 - Atomic population in the excited state.

F_n - Amplifier noise figure.

β - Propagation constant.

τ_g - Group delay.

v_g - Group velocity.

β_2 - Group velocity dispersion.

D - Dispersion parameter.

Δ_τ - Differential group delay.

D_{PMD} - PMD parameter of the fiber.

$i_I(t), i_Q(t)$ - Photodetector outputs.

R - Responsivity factor.

c - Speed of light.

τ - Time delay.

τ_{err} - Timing phase error.

y_1, y_2 - MIMO outputs.

$E(.)$ - Statistical expectation operation.

ε - Error signal.

μ - Convergence parameter.

Δf - Frequency offset.

T_{samp} - Time between samples.

R_k - Closest constellation radius.

σ^2 - Variance.

$erfc$ - Complementary error function.

H - 3 dB coupler transfer function.

C - Covariance matrix.

ϕ_{est} - Phase error estimate.

B_{ref} - Reference bandwidth.

R_s - Symbol rate.

p - Number of polarizations/orientations.

Contents

1 Introduction

1.1 Context

The invention of optical fibers in the 1970s vastly improved the field of telecommunications. The high bandwidth capability of optical fibers is an attractive characteristic, supporting the transmission of high volumes of information with low attenuation. The recent developments in digital coherent detection technology in optical communication systems enabled the transmission of high-order M-ary quadrature amplitude modulation (QAM) formats (16-QAM, 32-QAM, 64-QAM, and 256-QAM) in high-speed coherent optical transmission systems (MORI *et al.*, 2008) (FREUND *et al.*, 2011)(COELHO; HANIK, 2005). Indeed, high-order QAM transmission increases the data rate in a limited bandwidth (ZHOU; YU, 2009a), increasing capacity and reducing the requirements on analog-to-digital converters (ADC) (PFAU *et al.*, 2009). However, these modulation formats are more susceptible to laser phase noise because of their smaller Euclidean distance between the constellation points (ZHOU; YU, 2009b). The recent combination of coherent detection with digital signal processing (DSP) compensates impairments like chromatic dispersion and polarization mode dispersion. In addition, phase noise generated by the transmitter and local oscillators lasers, needs to be compensated, as it leads to symbol detection errors and affects the overall system performance. Therefore, carrier phase recovery is an indispensable function in coherent optical communication systems.

Phase recovery algorithms have been recently investigated extensively in the context of coherent optical communications (ZHOU, 2010; DRIS *et al.*, 2013; VITERBI, 1983). Phase recovery methods are mainly classified into two types: feedback and feedforward. Feedback approaches use the phase noise estimates of previous symbols to compensate the phase noise of the current symbol. In contrast, the feedforward approaches can track the phase of the transmitted signal without resorting to previous estimates. In general, feedforward techniques are preferred for allowing parallelization (WU; SUN, 2012). Some simple phase recovery algorithms, designed for 4-QAM signals, were presented in (IP A. LAU; KAHN, 2008; CHARLET *et al.*, 2009), being the Viterbi and Viterbi algorithm (SAVORY, 2010) one of the most simple solutions. In addition, several phase recovery algorithms for high-order modulation formats have been proposed, resorting to a decision-directed feedback loop (IP; KAHN, 2007; LOUCHET *et al.*, 2008; TARIGHAT *et al.*, 2006), or using feedforward approaches (SEIMETZ, 2008) (PFAU *et al.*, 2009). Among several proposals, the BPS algorithm (PFAU *et al.*, 2009) emerged as a de-facto standard for the recovery of M-QAM constellations. Compared to decision-directed schemes, the

BPS algorithm has the advantage of making decisions after rotations with test phases. This circumvents the effect of propagating erroneous decisions which severely impact the system performance, particularly at high error rates. BPS uses filtering of neighboring samples to mitigate the impact of additive noise and improve phase noise tracking. In addition to this, BPS is suitable for pipeline implementations.

The performance of phase recovery algorithms is usually evaluated by the signal to noise ratio (SNR) required to achieve a BER of 10^{-3} for a given $\Delta\nu T_s$ product, where $\Delta\nu$ is the sum of receiver and transmitter laser linewidths, and T_s is the symbol period (PFAU *et al.*, 2009). However, with the evolution of variable-rate error-correction schemes and the deployment of coded modulation (MELLO *et al.*, 2014), pre-FEC error rates in the order of 10^{-2} and higher have been considered (SALES *et al.*, 2017). At the same time, the $\Delta\nu T_s$ product has decreased, thanks to ever-increasing symbol rates. At low phase noise and high additive noise conditions, as it is usually the case at $> 10^{-2}$ pre-FEC BERs, the optimum window length of BPS can reach hundreds of symbols. This is far higher than the degree of parallelism of current ASIC implementations, requiring several long registers to implement filtering without excessively increasing the chip area. Recent adaptations to the BPS (NAVARRO *et al.*, 2017; ROZENTAL *et al.*, 2017; ZHUGE *et al.*, 2011) attempt to optimize the number and quality of test phases, reducing complexity, but the noise-rejecting filters remain long.

1.2 Contribution

This thesis proposes a modified BPS architecture for phase recovery of M-QAM constellations. The algorithm replaces the long filters used for BPS at low SNRs by a recursive architecture using a forgetting factor. BPS has been the preferred choice because its complexity has a weak dependency on the degree of parallelism, but it has a strong dependency on the error rate. Alternatively, the complexity of the recursive architecture implemented in pipeline has a weak dependency on the error rate, but a strong dependency on the degree of parallelism. Accordingly, filtering noise with forgetting factors is equivalent to using infinite windows with exponentially decaying coefficients. There are several architectures for implementing recursive filters in pipeline, corresponding to different trade-offs between latency and number of operations (PARHI; MESSERSCHMITT, 1989). Potential gains with the proposed algorithm would depend strongly on the implementation architecture, level of parallelization and amount of additive noise. Therefore, we do not attain to any specific implementation method and restrict ourselves in analyzing the system performance. The forgetting factor BPS (FF-BPS) method is validated using simulations and experiments carried out under practical operating conditions. The

performance of this method is evaluated for 16-QAM and 64-QAM constellations based on an optical signal to noise ratio (OSNR) penalty at BER = 10^{-3} and compared with the performance of the BPS and DD algorithms.

The remainder of this thesis is structured as follows. Chapter 2 describes the transmission and reception of the signals through coherent optical communication systems and commonly deployed signal processing algorithms. Chapter 3 describes the effect of phase noise during signal transmission and details the most common phase recovery algorithms used in coherent optical communication. This includes the description of the proposed FF-BPS algorithm. Chapter 4 describes the simulation setup and experimental results. Finally, Chapter 5 concludes the thesis.

1.3 Associated Publications

Aparna Aravind Payyazhi, André Luiz Nunes de Souza, Darli Augusto de Arruda Mello. "Recursive blind phase search architecture for phase recovery at high error rates". In Proc. of SBFoton International Conference, 2018, Campinas, pp.1-5.

2 Coherent Optical Communications Systems

An optical communication system contains a set of elements for transmitting and receiving information, having the optical fiber as a waveguide. Fig. 2.1 shows a simplified block diagram of the optical communication system. The input data is fed into the transmitter, which converts the electrical signal into the optical domain. The channel comprises the optical fiber and all other optical components. Finally, the receiver converts the input signal to the electrical domain and recovers the transmitted information. The next sections provide a brief overview of these blocks.

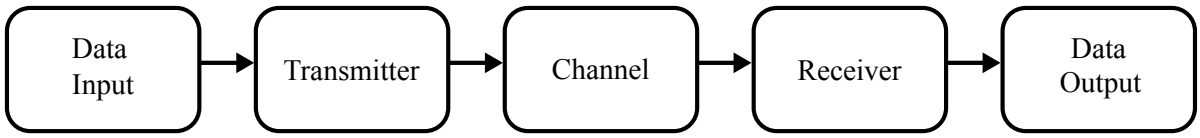

Figure 2.1 – Block diagram of optical communication system.

2.1 Transmitter

The transmitter block receives input bit sequences and maps them into the desired constellation according to a specified modulation format. Among several options, the quadrature amplitude modulation (QAM) scheme is widely used in optical receivers. It modulates the amplitude of the carrier signals using amplitude-shift keying (ASK) applied independently in the in-phase and quadrature components. QAM with suitable constellation sizes can achieve high spectral efficiencies, however, its performance is limited by the noise level and linearity of the communication channel. Fig. 2.2 shows the constellation diagram of typical M-QAM modulation formats. In particular, this thesis investigates the 16-QAM and 64-QAM formats, which are important candidates for future generation optical systems.

After the modulation format is generated in the electrical domain, it must be translated into the optical domain. Optical modulation can be classified into direct and external. In direct modulation, the incoming signal modulates directly the feed current of the laser source. In contrast, in external modulation, a separate device, called a modulator, is required. Compared with direct modulation, external modulation is faster and mitigates the impact of chirp. However, due to the usage of the external device, it tends to be more expensive.

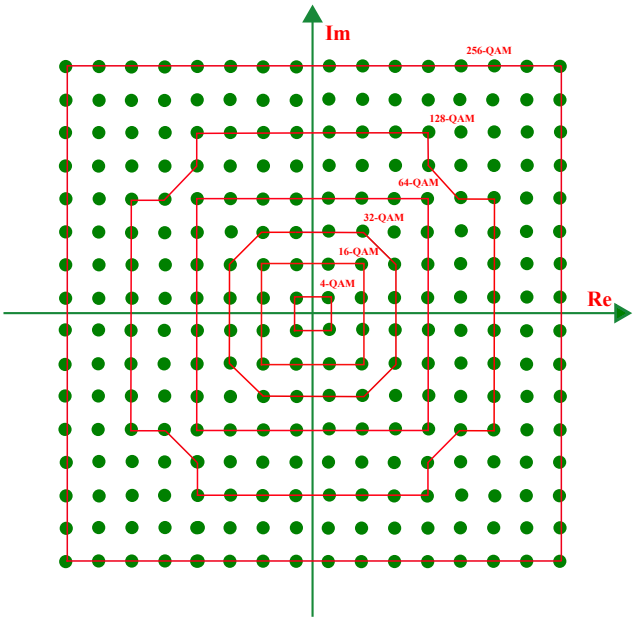

Figure 2.2 – M-QAM constellation diagram.

Coherent optical systems operate with external modulation using Mach-Zehnder modulators (MZM), whose basic architecture is shown in Fig. 2.3. It consists of two phase modulators that are assembled in each of the two arms. The input light signal is distributed into two phase modulators, where a phase difference is generated. After that, the two optical fields are recombined.

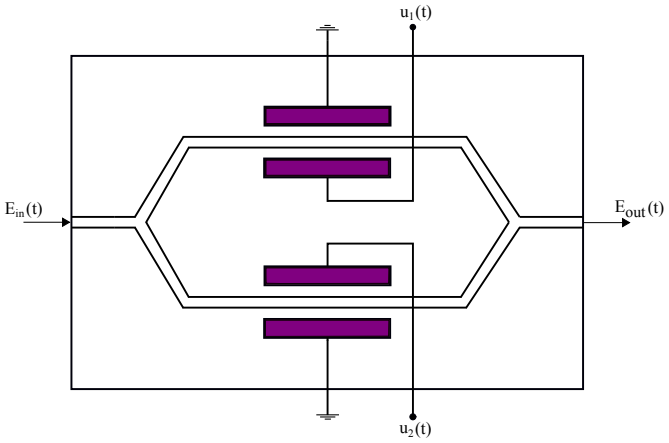

Figure 2.3 – Mach-Zehnder modulator.

According to the phase deviation imprinted in the two arms, the interference pattern at the end of the modulator changes from constructive to destructive. The transfer function of the MZM, without insertion losses, is given as (MATTHIAS; SEIMETZ, 2009):

$$\frac{E_{out}(t)}{E_{in}(t)} = \frac{1}{2}(e^{j\phi_1(t)} + e^{j\phi_2(t)}) \tag{2.1}$$

where $E_{out}(t)$ and $E_{in}(t)$ are output and input electric fields, $\phi_1(t)$ and $\phi_2(t)$ are the phase shifts introduced in the two arms of the MZM. The equation which relates the phase shifts and the driving voltages $u_1(t)$ and $u_2(t)$ is given by (MATTHIAS; SEIMETZ, 2009):

$$\phi_1(t) = \frac{u_1(t)}{V_{\pi_1}}\pi \tag{2.2}$$

$$\phi_2(t) = \frac{u_2(t)}{V_{\pi_2}}\pi \tag{2.3}$$

where V_{π_1} and V_{π_2} are the voltages required to achieve the phase shift of π. If the phase shift $\phi(t) = \phi_1(t) = \phi_2(t)$, then the MZM is said to operate in push-push mode. In this condition, the MZM acts like a simple phase modulator (PM). The relation between input and output electric fields can be represented as (MATTHIAS; SEIMETZ, 2009):

$$E_{out}(t) = E_{in}(t)e^{j\phi_{PM}(t)} = E_{in}(t)e^{j\frac{u(t)}{V_\pi}\pi} \tag{2.4}$$

If $\phi_1(t) = -\phi_2(t)$, $u_1(t) = -u_2(t) = u(t)/2$ and $V_{\pi_1} = V_{\pi_2} = V_\pi$, the MZM operates in push-pull mode, and the modulated output does not have chirp. In this case, we can represent the relation between input and output electric fields as (MATTHIAS; SEIMETZ, 2009):

$$E_{out}(t) = E_{in}(t)\cos\left(\frac{\Delta\phi(t)}{2}\right) = E_{in}(t)\cos\left(\frac{u(t)}{2V_\pi}\pi\right) \tag{2.5}$$

where $\Delta\phi(t) = \phi_1(t) - \phi_2(t)$. The MZM in push-pull mode produces an optical field which can be modulated in amplitude and polarity, i.e., its phase can be switched between $-\pi$ and π rad. The power transfer function of MZM is represented as (MATTHIAS; SEIMETZ, 2009):

$$\frac{P_{out}(t)}{P_{in}(t)} = \frac{1}{2} + \frac{1}{2}\cos\left(\frac{u(t)}{V_\pi}\pi\right) \tag{2.6}$$

Fig. 2.4 shows the output of MZM which operates at the minimum transmission point. When the MZM operates at the minimum transmission point with a DC bias of V_π, there is an excursion of input signal occurs from $-2V_\pi$ and 0. This method is used for the generation of the pulse amplitude modulation (PAM) signals.

QAM formats are usually generated by in-phase and quadrature modulators (IQM), which comprise two push-pull MZM modulators and a phase modulator. The IQM is assembled with one MZM in each of the two arms, and the phase modulator is located in the lower arm, as shown in Fig. 2.5. Here, $E_{in}(t)$ and $E_s(t)$ are the input and output electric fields, and $V_1(t)$, $V_2(t)$, and V_3 are the driving voltages of the three MZMs.

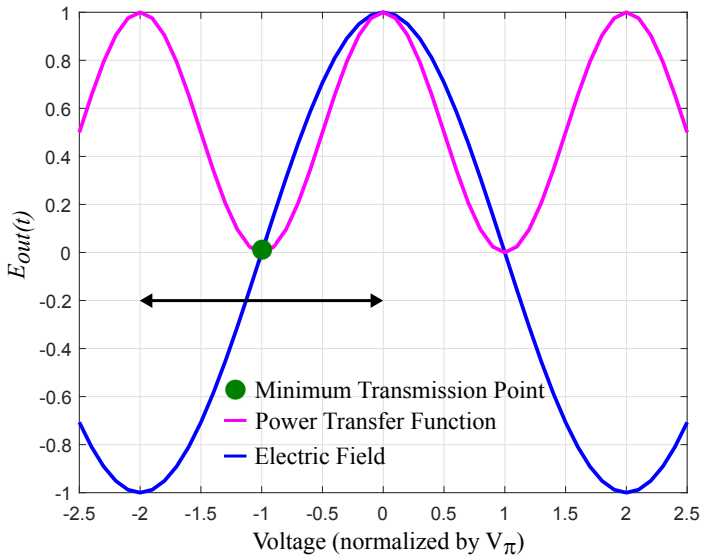

Figure 2.4 – Operation of MZM at the minimum transmission point.

The relation between the input electric field and output electric field is given by (ROUDAS; IOANNIS, 2012):

$$E_s(t) = \frac{1}{2}\left[\cos\left(\frac{\pi V_1(t)}{2V_{\pi_1}}\right) + e^{j\frac{\pi V_3}{V_{\pi_3}}}\cos\left(\frac{\pi V_2(t)}{2V_{\pi_2}}\right)\right] E_{in}(t) \tag{2.7}$$

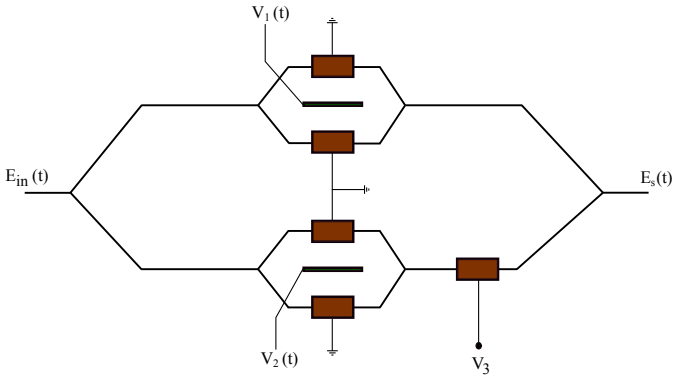

Figure 2.5 – In-phase and quadrature modulator (IQM).

2.2 The Optical Channel

The optical channel provides a connection between the transmitter and the receiver. It includes effects generated at the optical fiber as well as at the components traversed by the optical signals, such as amplifiers. The next sections present the basics of some fundamental effects that affect the optical channel propagation.

2.2.1 Signal Attenuation

Attenuation is a phenomenon related to intrinsic losses of the optical power along the propagation through the optical fiber. The equation which relates the average optical power P and the propagation distance Z is given by (AGRAWAL, 2002):

$$\frac{dP}{dZ} = -\alpha P \tag{2.8}$$

where α is the attenuation coefficient. From the above equation, the output and input powers P_{out} and P_{in} are related by:

$$P_{out} = P_{in}e^{-\alpha L} \tag{2.9}$$

where L is the fiber length. The attenuation coefficient in dB/km is given as (AGRAWAL, 2002):

$$\alpha \left[\frac{dB}{km}\right] = \frac{-10}{L} log_{10}\left(\frac{P_{out}}{P_{in}}\right) \approx 4.343\alpha \left[\frac{Np}{km}\right] \tag{2.10}$$

Fiber losses are mainly due to material absorption and scattering. Material absorption is caused by impurities like Fe, Ni, Co, and Al, and infra-red absorption. Also, the OH^- molecule absorbs light. Rayleigh scattering is a phenomenon which is generated because of perturbations in the refractive index of the optical fiber due to density fluctuations. Fig. 2.6 represents the various types of signal attenuation occurring in the optical fiber.

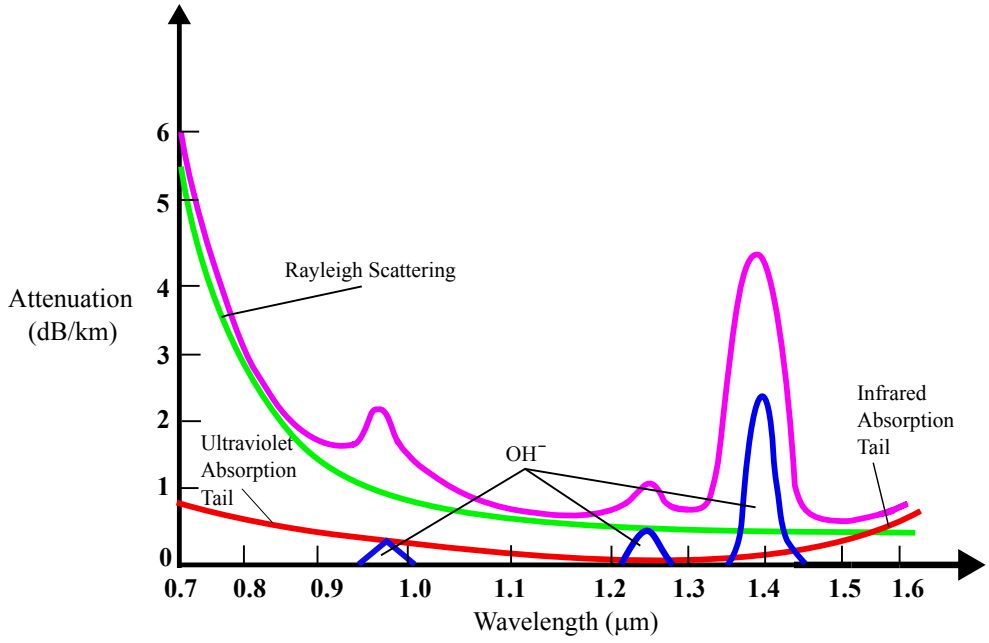

Figure 2.6 – Contribution of different phenomena to fiber losses. Adapted from (HENTSCHEL, 1983).

2.2.2 Amplified Spontaneous Emission (ASE) Noise

The spontaneous emission of radiation is a process in which atoms decay from a higher energy level to a lower energy level by emitting a photon without any external triggering event. In this case, the emitted photons have random direction, polarization, and phase (RAMASWAMI; SIVARAJAN, 2002). On the other hand, the stimulated emission process requires external radiation for stimulating the transition of atoms from higher energy levels to lower energy levels. Unlike spontaneous emission, the emitted photon and incident photon have the same frequency, phase, direction of propagation, and polarization. Amplifiers use the stimulated emission process for signal amplification (RAMASWAMI; SIVARAJAN, 2002). The amplifier also considers the spontaneous emission of radiation itself as incident signal and amplifies it. This leads to the generation of amplified spontaneous emission (ASE) noise at the output of the amplifier and degrades SNR. The power of ASE noise at the output of the amplifier can be written as (RAMASWAMI; SIVARAJAN, 2002):

$$P_N = n_{sp} h f_c (G-1) B_o \tag{2.11}$$

where n_{sp} is the spontaneous emission factor (population-inversion factor), G is the amplifier gain, and B_o is the optical bandwidth, and h the Planck's constant. The spontaneous emission factor is given by (AGRAWAL, 2002):

$$n_{sp} = N_2/(N_2 - N_1) \tag{2.12}$$

where N_1 is the atomic population in the ground state and N_2 is the atomic population in the excited state. One of the most important parameters of an amplifier is its noise figure F_n, which in optical systems is usually approximated by (AGRAWAL, 2002):

$$F_n \approx 2 n_{sp} \tag{2.13}$$

2.2.3 Fiber Dispersion

Chromatic dispersion (CD) is a linear fiber effect that broadens pulses launched into optical fibers, leading to inter-symbol interference (BORKOWSKI *et al.*, 2014). It arises from the fact that different spectral components of the optical pulse travel with different group velocities over the fiber, spreading pulses, as shown in Fig. 2.7. In this figure, initially, at time t_1, two input pulses are separate. After some distance of propagation (time $t_2 > t_1$) the amplitude of the pulses reduces a little. Again, at the time $t_3 > t_2$, the amplitude of the pulses reduces more and the pulses become barely distinguishable.

Finally, at the time $t_4 > t_3$, the amplitude of the pulses reduces considerably and one pulse cannot be distinguished from another due to pulse broadening.

Chromatic dispersion has two main origins, called material dispersion and waveguide dispersion. Material dispersion arises in optical fibers from the silica properties. In contrast, waveguide dispersion is generated by the power distribution of signal propagating between core and cladding. Chromatic dispersion is usually quantified by the second derivative of the mode phase constant β around frequency ω_0 (NAVARRO, 2017):

$$\beta(\omega) = \beta(\omega_0) + \left(\frac{d\beta}{d\omega}\right)(\omega - \omega_0) + \frac{1}{2}\left(\frac{d^2\beta}{d\omega^2}\right)(\omega - \omega_0)^2 + \frac{1}{6}\left(\frac{d^3\beta}{d\omega^3}\right)(\omega - \omega_0)^3 + \ldots \quad (2.14)$$

Chromatic dispersion is related to term $\frac{d^2\beta}{d\omega^2} = \beta_2$, called group velocity dispersion (GVD) parameter. A more common metric used to quantify chromatic dispersion is the dispersion parameter D, which can be represented as (AGRAWAL, 2002):

$$D = \frac{d}{d\lambda}\left(\frac{1}{v_g}\right) = \frac{-2\pi c}{\lambda^2}\beta_2 \quad (2.15)$$

where v_g is the group velocity, λ is the operating wavelength and c is the speed of light. The fiber dispersion transfer function can be obtained by discarding the terms of the Eq. 2.14 beyond the second and which is represented as (SHARIFIAN, 2010):

$$H(\omega) = exp\left(-j\frac{\beta_2 L}{2}\omega^2\right) = exp\left(j\frac{D\lambda^2 L}{4\pi c}\omega^2\right) \quad (2.16)$$

where L is the fiber length.

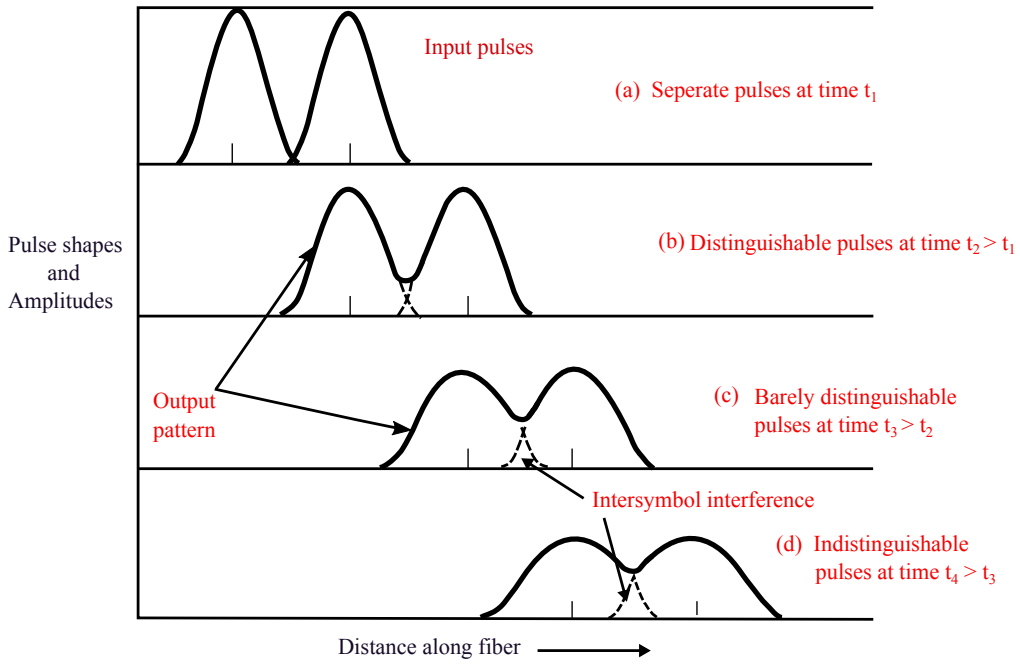

Figure 2.7 – Spread of pulses due to fiber dispersion. Adapted from (KEISER, 1991).

2.2.4 Polarization Mode Dispersion (PMD)

PMD occurs mainly due to perturbations in the shape of the fiber core, acquiring an elliptical shape because of mechanical and thermal stresses. These perturbations cause fiber birefringence, i.e., pulses launched in the two orthogonal polarization components travel at different group velocities. Hence, one polarization component travels faster than the other, which causes a propagation time difference (DAMASK, 2005) called differential group delay (DGD) (NELSON; JOPSON, 2005) (see Fig. 2.8). Initially, the horizontal and vertical polarization components of the input pulse travel at the same group velocities and after propagation through an optical fiber, the two polarization components travel at different group velocities due to the birefringence. The DGD is usually expressed as:

$$\Delta\tau = D_{\mathrm{PMD}}\sqrt{L} \tag{2.17}$$

where $\Delta\tau$ is the differential droup delay, L is the fiber length, and D_{PMD} is the PMD parameter of the fiber. Note that the DGD depends on the square root of L, mainly because of the random nature of fiber ellipticity.

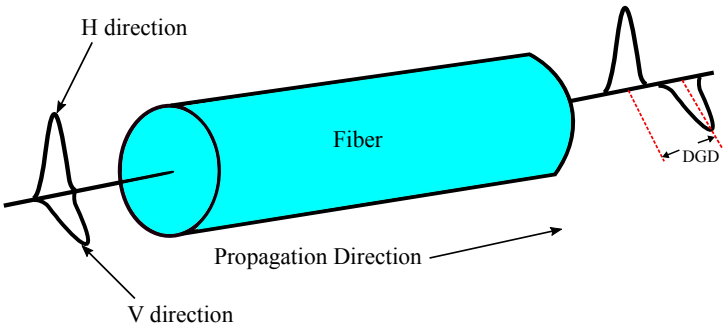

Figure 2.8 – Polarization mode dispersion. Adapted from (GALTAROSSA, 2005).

2.2.5 Nonlinearities

At high fiber launch powers, the optical fiber operates in a nonlinear regime, generating distortions that strongly impair the signal quality. These nonlinearities as produced by different effects, particularly nonlinear scattering and nonlinear phase modulation. These effects are not addressed in the thesis as, in general, they are not compensated for in coherent receivers.

2.3 Coherent Receiver

The receiver block retrieves the signal from the optical channel and converts it into the electrical domain. This work is concerned with coherent receivers, which resort

to local oscillators to track the phase of the received signal and recover amplitude- and phase-modulated signals. Coherent receivers can be classified into homodyne and heterodyne. In homodyne receivers, the frequency of the local oscillator laser is the same as that of the transmitter laser, whereas in heterodyne receivers the local oscillator and transmitter lasers differ by an intermediate frequency (IF). Optical coherent receivers accomplish a quasi-homodyne detection (sometimes called intradyne), where a small mismatch between transmitted and local oscillator lasers are compensated for using signal processing algorithms.

In general terms, the optical coherent receivers can be divided into a front-end, responsible for the optoelectrical conversion, followed by a chain of signal processing algorithms that recover the transmitted information. Fig. 2.9 shows the schematic diagram of a chain of coherent receiver DSP algorithms. The brief description of the blocks is included in the following section.

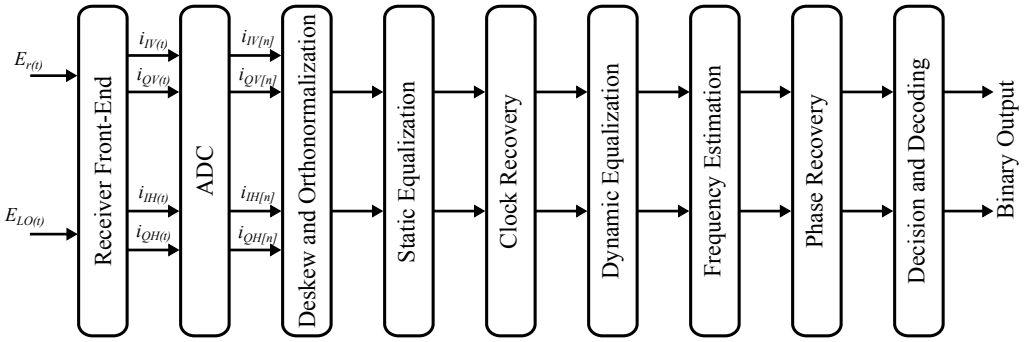

Figure 2.9 – Chain of coherent receiver DSP algorithms.

2.3.1 The Receiver Front-end

Fig. 2.10 shows the homodyne receiver front-end commonly used in optical communications (IP A. LAU; KAHN, 2008). It consists of a local oscillator, four 3-dB couplers, and four photodetector diodes (or two balanced photodetectors), in addition to a phase shifter.

The 3-dB coupler is a 2×2 coupler (two input ports and two output ports) that splits the input power equally to the outputs (AGRAWAL, 2002). After an input stage composed of two 3-dB couplers and a 90 degrees phase shifter, there is an output stage composed of two couplers. In the following, the outputs of the first output coupler are represented as E_1 and E_2, and the outputs of the second output coupler are represented as E_3 and E_4, as indicated in Fig. 2.10. The photocurrents generated at the output of the balanced photodetectors $i_I(t)$ and $i_Q(t)$ correspond to in-phase and quadrature components of the input optical signal. Transfer function of 3-dB coupler is given as (HO, 2005):

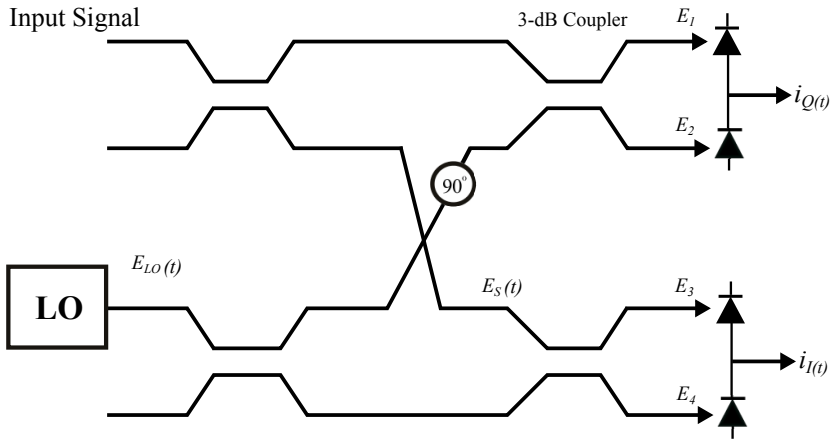

Figure 2.10 – Homodyne receiver for a single-polarization system.

$$H = \frac{1}{\sqrt{2}} \begin{bmatrix} 1 & 1 \\ 1 & -1 \end{bmatrix} \tag{2.18}$$

Output electric fields E_1, E_2, E_3, and E_4 can be obtained by using the above represented transfer function (KIKUCHI, 2010):

$$E_1 = \frac{1}{2}(E_s + jE_{LO}) \tag{2.19}$$

$$E_2 = \frac{1}{2}(E_s - jE_{LO}) \tag{2.20}$$

$$E_3 = \frac{1}{2}(E_s + E_{LO}) \tag{2.21}$$

$$E_4 = \frac{1}{2}(E_s - E_{LO}) \tag{2.22}$$

The photodetectors are optoelectronic devices, which converts the optical signals into electrical signals. It generates a current I_p corresponding to the input power P_{in} expressed as (RAMASWAMI; SIVARAJAN, 2002):

$$I_p = RP_{in} \tag{2.23}$$

where R represents the responsivity factor. Based on the above equation the photocurrents obtained for in-phase and quadrature components can be written as:

$$i_Q(t) = i_1(t) - i_2(t) = R|E_1|^2 - R|E_2|^2 \tag{2.24}$$

$$i_I(t) = i_3(t) - i_4(t) = R|E_3|^2 - R|E_4|^2 \tag{2.25}$$

Substitute the Eqs. 2.19 - 2.22 in Eqs. 2.24 and 2.25, resulting:

$$i_Q(t) = R|\frac{1}{2}(E_s + jE_{LO})|^2 - R|\frac{1}{2}(E_s - jE_{LO})|^2 \tag{2.26}$$

$$i_I(t) = R|\frac{1}{2}(E_s + E_{LO})|^2 - R|\frac{1}{2}(E_s - E_{LO})|^2 \tag{2.27}$$

For optical systems with polarization multiplexing, the receiver front-end architecture replicates the single polarization with the aid of polarization beam splitters, as shown in Fig. 2.11.

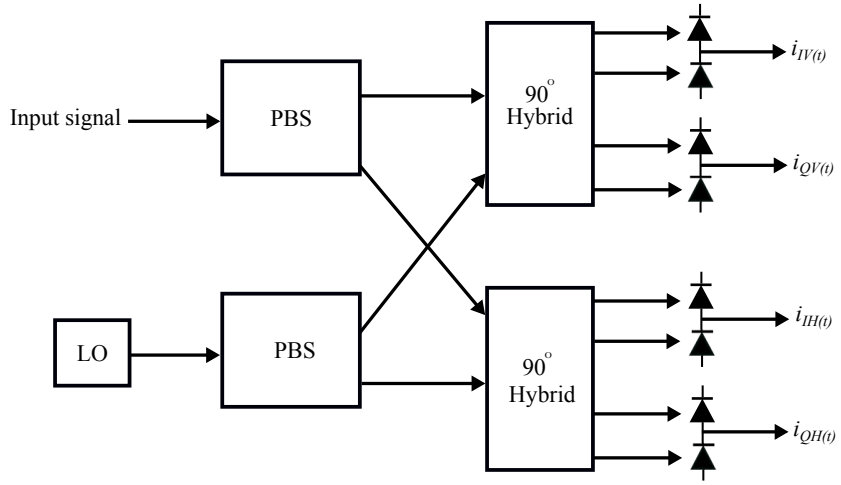

Figure 2.11 – Receiver front-end for a dual-polarization system.

After opto-electrical conversion the received signals are sent to a set of analog-to-digital converters (ADCs) for subsequent digital signal processing (SAVORY, 2010).

2.3.2 Digital Signal Processing (DSP) Algorithms

After the receiver front-end, the signals are treated by a chain of signal processing algorithms. This thesis focus on phase recovery, which will be presented with more detail in the following chapter. For the sake of completeness, we next describe shortly the remaining algorithms.

Deskew and orthonormalization

The DSP algorithms are mainly used for compensating the impairments that are induced during the transmission and reception of the signals. The first two tasks of the chain of DSP algorithms is to compensate for imperfections generated in the front-end of the coherent receiver. Due to mismatches of the path length between the in-phase and quadrature channels of the received signals, there can be a lack of time synchronization between the signals (SAVORY, 2010) leading to a time delay called skew. To compensate for these delays, interpolation-based deskew algorithms are usually implemented. The implementation of an interpolator can be done by using a finite-impulse-response (FIR) filter (TANIMURA *et al.*, 2009). Another front-end imperfection that must be compensated is that responsible for imbalances in the in-phase and quadrature (IQ) components of the received signals (AL-MAJMAIE, 2014). Orthonormalization algorithms are used

to compensate for these IQ imbalances, being the Gram-Schmidt orthogonalization and the Löwdin orthogonalization (SAVORY, 2010) the most common solutions. Consider the complex signal with imbalances as having in-phase and quadrature components $I'(t)$ and $Q'(t)$ (FARUK; SAVORY, 2017). The mathematical expression for the Gram-Schmidt orthogonalization method is (FARUK; SAVORY, 2017):

$$\begin{bmatrix} I(t) \\ Q(t) \end{bmatrix} = \begin{bmatrix} 1 & 0 \\ -a & 1 \end{bmatrix} \begin{bmatrix} I'(t) \\ Q'(t) \end{bmatrix} \tag{2.28}$$

where a is the inner product between I' and Q', and I and Q are the decorrelated components. As shown in Fig. 2.12a, the method rotates the quadrature component to make in-phase and quadrature components orthogonal to each other. On the other hand, the Löwdin orthogonalization method rotates both vectors by the same angle and makes them orthogonal, as shown in Fig. 2.12b. The method can be represented mathematically by (FARUK; SAVORY, 2017):

$$\begin{bmatrix} I(t) \\ Q(t) \end{bmatrix} = \frac{1}{2} \begin{bmatrix} 1/\sqrt{(1+a)} + 1/\sqrt{(1-a)} & 1/\sqrt{(1+a)} - 1/\sqrt{(1-a)} \\ 1/\sqrt{(1+a)} - 1/\sqrt{(1-a)} & 1/\sqrt{(1+a)} + 1/\sqrt{(1-a)} \end{bmatrix} \begin{bmatrix} I'(t) \\ Q'(t) \end{bmatrix} \tag{2.29}$$

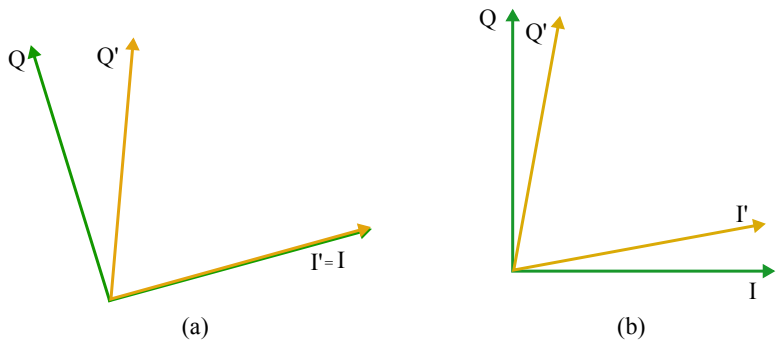

Figure 2.12 – (a) Gram-Schmidt and (b) Löwdin orthogonalization algorithms.

Static Equalization

The static equalizer compensates for chromatic dispersion by using large filters with pre-computed coefficients (SAVORY, 2010). Its implementation is carried out using the inverse response of the fiber dispersion transfer function. Generally, FIR filters with inverse chromatic dispersion transfer function implemented in the frequency domain are used for compensating the chromatic dispersion (KUSCHNEROV *et al.*, 2009) (BORKOWSKI *et al.*, 2014). Based on the Eq. 2.16, the frequency response of the inverse

chromatic dispersion filter can be expressed as (SHARIFIAN, 2010):

$$H_{icd}(\omega) = exp\left(j\frac{\beta_2 L}{2}\omega^2\right) \tag{2.30}$$

Clock Recovery

The main function of the clock recovery subsystem is to correct the differences in timing phase and frequency between the transmitter and receiver clock. One of the most common methods used for timing recovery is the Gardner algorithm. The timing phase error τ_{err} according to Gardner algorithm is given as (FARUK; SAVORY, 2017):

$$\tau_{err} = Re\left[\sum_{n=0}^{N/2-1}\left[x_i(2n-1) - x_i(2n+1)\right]x_i^*(2n)\right] \tag{2.31}$$

where $x_i(n)$ is the complex input signal and N is the number of samples. The Gardner's method in the frequency domain is given by (FARUK; SAVORY, 2017):

$$\tau_{err} = \sum_{k=0}^{N/2-1} Im\left[X_i(k)X_i^*(k+N/2)\right] \tag{2.32}$$

in which $X_i(k)$ is DFT of $x_i(n)$.

Dynamic Equalization

The dynamic equalization is one of the main blocks of the chain of DSP of a coherent receiver, and will be described with more detail in this section. Multiple-input multiple-output (MIMO) adaptive equalizers are mainly used to compensate polarization-dependent effects and residual dispersion left over from the static equalizer. Their architecture is shown in Fig. 2.13.

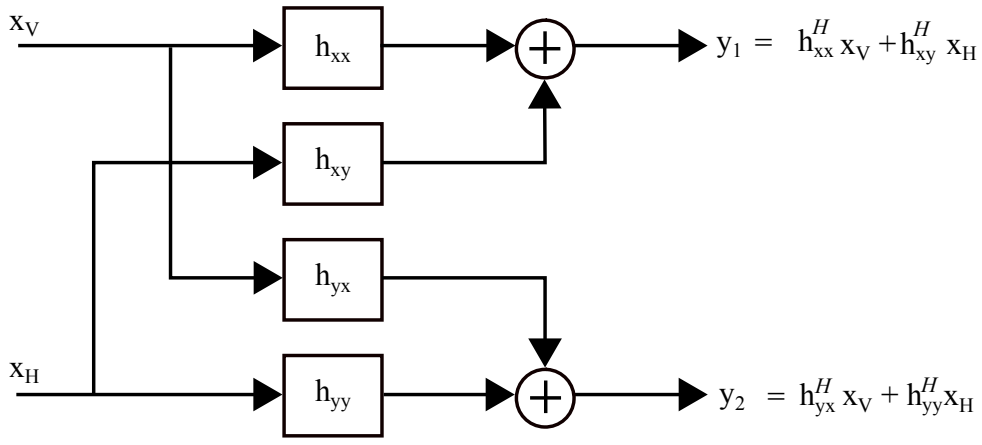

Figure 2.13 – MIMO equalizer.

The typical MIMO equalizer of coherent optical receivers consists of four FIR filters displaced in the so-called butterfly structure. The output samples of the MIMO equalizer y_1 and y_2 can be represented as (SAVORY, 2010):

$$y_1[k] = \mathbf{h}_{xx}^H[k]\mathbf{x}_V[k] + \mathbf{h}_{xy}^H[k]\mathbf{x}_H[k] \tag{2.33}$$

$$y_2[k] = \mathbf{h}_{yx}^H[k]\mathbf{x}_V[k] + \mathbf{h}_{yy}^H[k]\mathbf{x}_H[k] \tag{2.34}$$

where $\mathbf{x}_V$ and $\mathbf{x}_H$ are vector inputs of the filter and $\mathbf{h}_{xx}$, $\mathbf{h}_{xy}$, $\mathbf{h}_{yx}$, and $\mathbf{h}_{yy}$ are the vector tap weights.

There are several algorithms to update the filter weights according to the channel conditions. Two of them are commonly used in optical communications. The first one is the constant modulus algorithm (CMA), introduced by Godard in (GODARD, 1980), which is suitable for constant-modulus modulation formats. The CMA tries to reduce the errors ε_x and ε_y based on stochastic gradient algorithm. The error signals are given by (SAVORY, 2010):

$$\varepsilon_x^2 = (1 - |y_1|^2)^2 \tag{2.35}$$

$$\varepsilon_y^2 = (1 - |y_2|^2)^2 \tag{2.36}$$

The update formula for the filters are given as (SAVORY, 2010):

$$\mathbf{h}_{xx} = \mathbf{h}_{xx} + \mu\varepsilon_x\mathbf{x}_V y_1^* \tag{2.37}$$

$$\mathbf{h}_{xy} = \mathbf{h}_{xy} + \mu\varepsilon_x\mathbf{x}_H y_1^* \tag{2.38}$$

$$\mathbf{h}_{yx} = \mathbf{h}_{yx} + \mu\varepsilon_y\mathbf{x}_V y_2^* \tag{2.39}$$

$$\mathbf{h}_{yy} = \mathbf{h}_{yy} + \mu\varepsilon_y\mathbf{x}_H y_2^* \tag{2.40}$$

where μ is the algorithm step size.

Although the CMA was designed for constant-modulus constellations, it still works for higher order QAM modulation formats, but with poor performance. Better results can be obtained with the radius-directed equalization (RDE) algorithm, whose error signal is given by (READY; GOOCH, 1990):

$$\varepsilon_x^2 = (R_k - |y_1|^2)^2 \tag{2.41}$$

$$\varepsilon_y^2 = (R_k - |y_2|^2)^2 \tag{2.42}$$

where R_k is the closest constellation radius.

Frequency Estimation

In an intradyne coherent receiver, the transmitter and local oscillator lasers do not operate at exactly the same frequencies. This leads to some residual frequency offset in the received signal which has to be compensated. The output of the dynamic equalizer can be represented as (FARUK; SAVORY, 2017):

$$y[k] = s[k]e^{j(\theta[k]+2\pi k\Delta f T_{samp})} + w[k] \tag{2.43}$$

where $s[k]$ is the transmitted signal, $\theta[k]$ is the phase noise, $w[k]$ is the additive white Gaussian noise (AWGN), Δf is the frequency offset introduced by the differences between operating frequencies of transmitter and local oscillator lasers and T_{samp} is the time between samples. The frequency estimation methods are mainly classified as blind and training-aided method (FARUK; SAVORY, 2017). Only blind estimation methods are described here. The time-domain differential phase based method is a blind estimation method in which the frequency offset is determined from the average phase increment of two consecutive symbols, represented as (LEVEN *et al.*, 2007):

$$\Delta\phi = 2\pi\Delta f T_{samp} \tag{2.44}$$

Fig. 2.14 shows the block diagram of the time-domain differential phase based method. In this method, the input signal $y(k)$ is first multiplied with the complex conjugate of the previous sample $y(k-1)$. Then, the Mth power of the resulting output is computed for removing the data dependency. In order to filter out noise, the results of several consecutive symbols are added. Finally, the argument of the summed values is calculated and divided by M. This method is easily applicable for M-ary PSK signals, however, it has poor performance in the case of high-order QAM because the high-order QAM contains only a small portion of the constellation points with equal phase spacing for extracting the frequency offset.

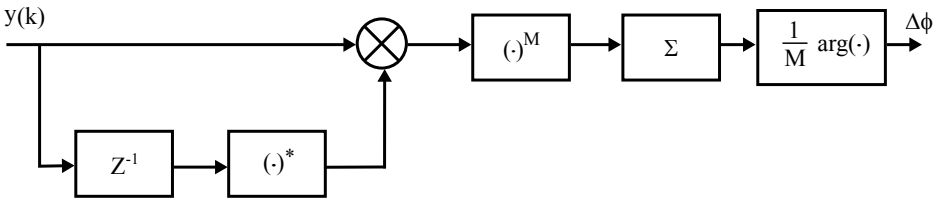

Figure 2.14 – Block diagram of time-domain differential phase based method.

Another commonly used blind estimation method is the frequency domain method, which is operated based on spectral analysis. In this method, Δf is determined

from a signal spectrum of M^{th} order, which exhibits a peak at the frequency of M times the frequency offset. The structure of this method is shown in Fig. 2.15.

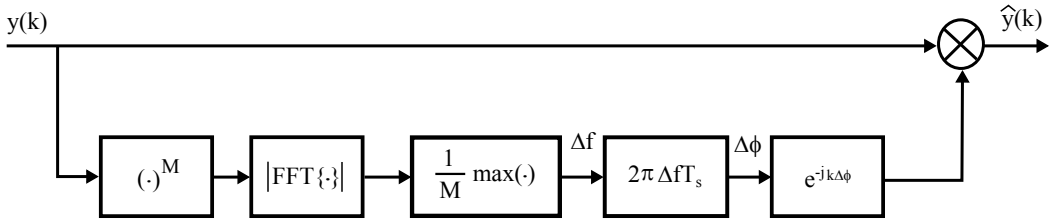

Figure 2.15 – Block diagram of frequency domain method.

The procedure of this method is the following. First, the M^{th} power of the input signal $y(k)$ is calculated for removing the information dependency of the transmitted signal. After that, the fast Fourier transform (FFT) of the obtained result is determined, and the frequency corresponding to its maximum value is divided by M for obtaining the frequency offset Δf. Finally, frequency correction is carried out as:

$$\hat{y}(k) = y(k)e^{-jk\Delta\phi} \tag{2.45}$$

The spectrum based method has better performance compared with the time-domain differential phase based method. However, it shows increased implementation complexity for high-order QAM signals (ZHOU, 2014).

Differential Encoding and Decoding

Differential encoding is a technique that encodes information in the difference between consecutive input signals. In this method, the transmitted data depends on the current and the previous signal state (NOE, 2005). Fig. 2.16 illustrates the basic concepts of the differential encoding and decoding processes. Here, changing the signal amplitude encodes a logical "1" bit, whereas maintaining its amplitude encodes a logical "0" bit. At the receiver, the original transmitted bit sequence is recovered by differential decoding.

High-order modulation formats are less tolerant to the laser phase noise. During detection, the presence of noise moves the current stable operating point of the estimate into a rotated stable operating point. This nonlinear phenomenon is called a cycle slip. In M-QAM modulation formats, cycle slips lead to errors due to a difference of $\pm\pi/2$ between the carrier and estimated phases. There are three different methods for detecting and correcting cycle slips (BARBOSA, 2017). One method is the differential encoding and decoding. The other one is non-data-aided and universal cycle slip detection and correction technique (GAO *et al.*, 2014). The third one is based on the soft-decision feedback

information from FEC decoder (KOIKE-AKINO *et al.*, 2014). In this work, cycle slips are corrected by differential encoding and decoding.

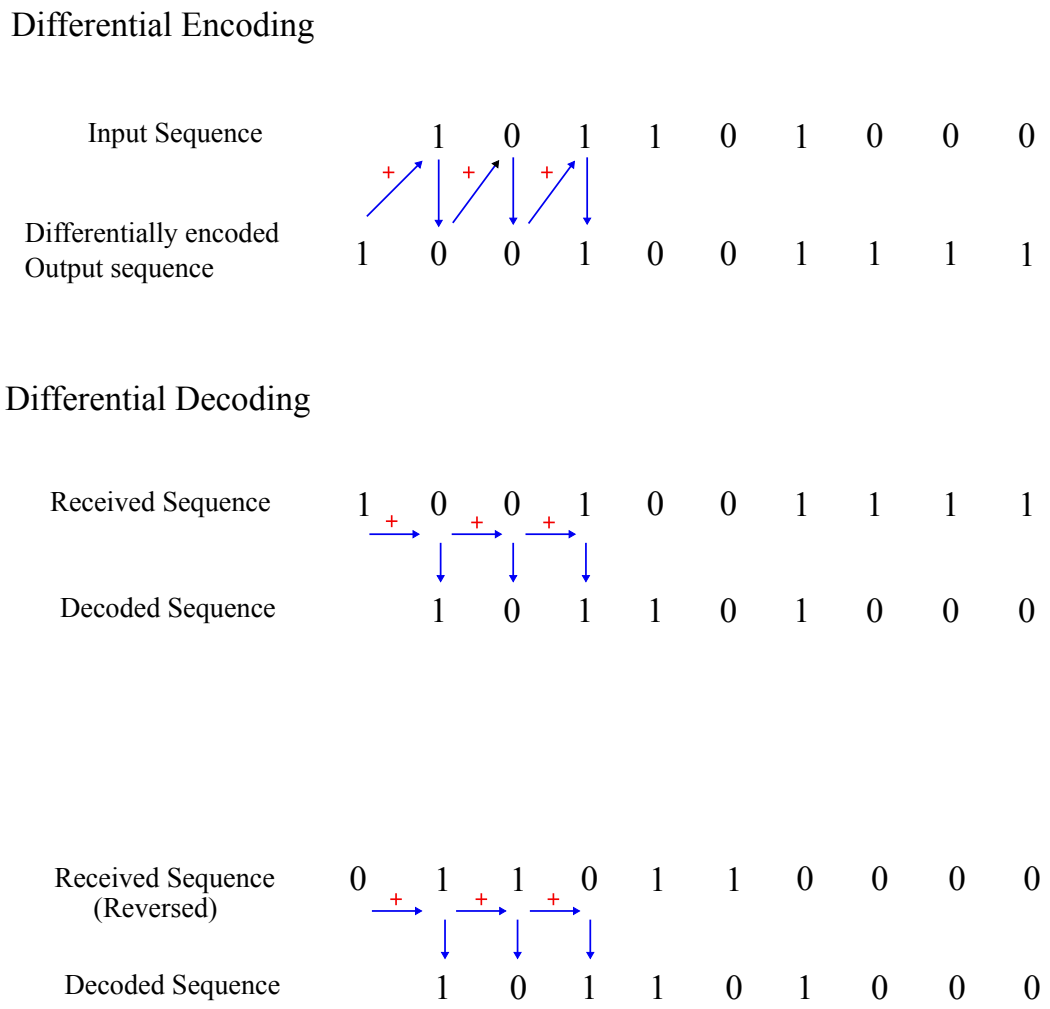

Figure 2.16 – Differential encoding and decoding process.

As an illustration, the differential encoding process for 16-QAM modulation format is schematically illustrated in the Fig. 2.17. The incoming bit sequence is divided into sets of four bits. In this set, the first two bits represent a modification in the quadrant (black arrows), and the last two bits represent the position of the bits within the quadrant (blue circles). The receiver performs the reverse process of differential decoding and detects the binary sequences.

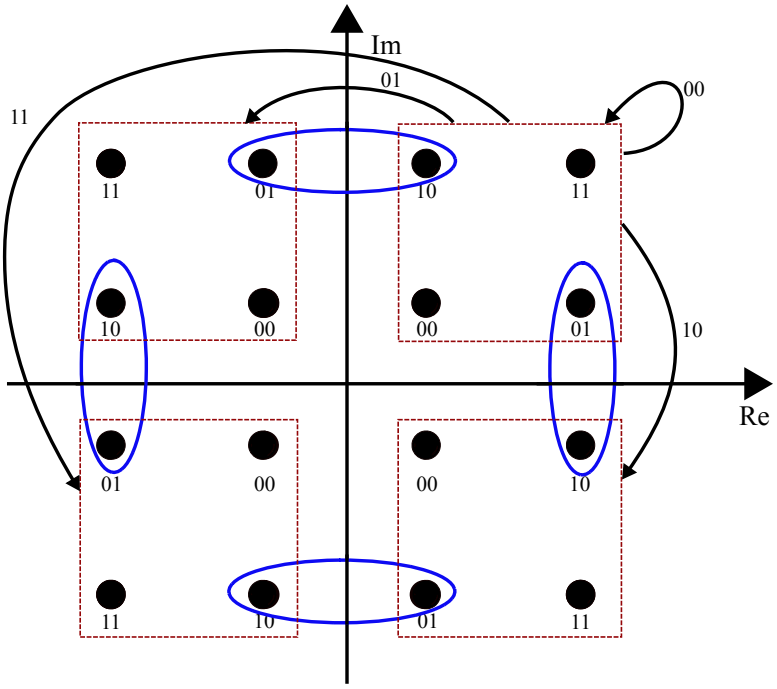

Figure 2.17 – 16-QAM bit to symbol mapping using differential encoding.

Fig. 2.18 shows the differential encoding process for 64-QAM. In this case, the procedures for differential encoding analogous as that of 16-QAM, except for the incoming bit sequence division. Here, two bits are used for quadrant encoding, whereas the remaining four bits determined a symbol within the quadrant.

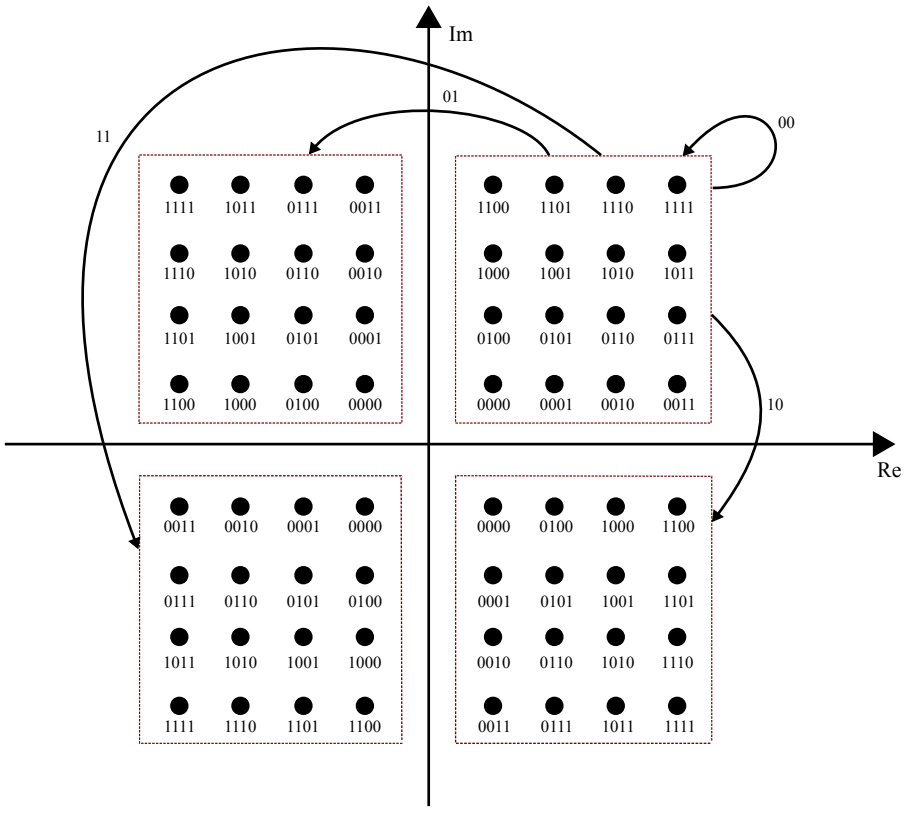

Figure 2.18 – 64-QAM bit to symbol mapping using differential encoding.

3 Phase Recovery in Coherent Optical Communication Systems

3.1 Phase Noise

Phase noise is an impairment generated by the transmitter and receiver lasers. It is well-modeled as a Wiener process (PFAU *et al.*, 2009), where the phase shift θ_k of the k^{th} symbol is represented as:

$$\theta_k = \theta_{k-1} + \Delta\theta_k \tag{3.1}$$

Here, $\Delta\theta_k$ is a Gaussian random variable with zero mean and variance:

$$\sigma_\Delta^2 = 2\pi\Delta\nu T_s \tag{3.2}$$

where $\Delta\nu$ is the sum of transmitter and local oscillator laser linewidths and T_s is the symbol duration. Thus, the kth received symbol, r_k, can be expressed as:

$$r_k = s_k e^{j\theta_k} + w_k \tag{3.3}$$

where s_k is the transmitted signal, w_k is the complex AWGN noise, and θ_k is the phase noise process. Fig. 3.1 shows phase noise realizations for different $\Delta\nu T_s$ values.

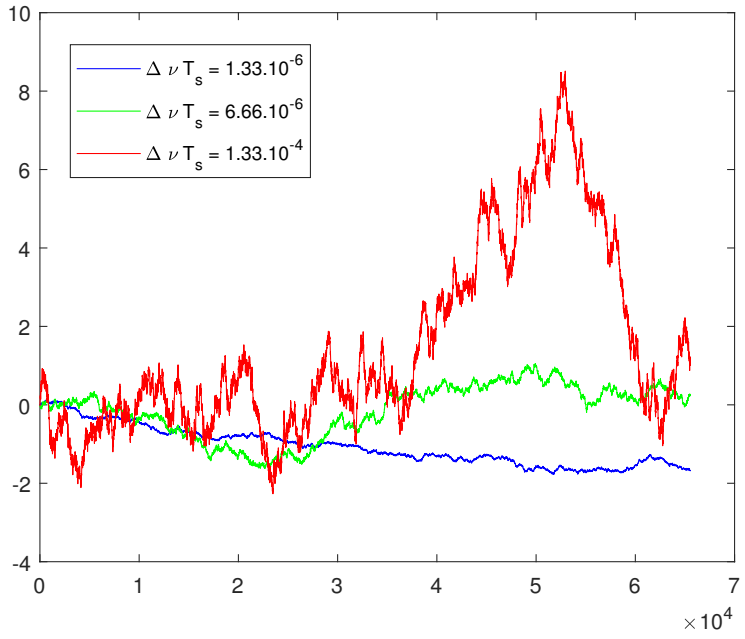

Figure 3.1 – Phase noise realizations for different $\Delta\nu T_s$. The considered symbol rate is 30 GBaud and the laser linewidths are 20 kHz, 100 kHz and 2 MHz.

Fig. 3.2 represents the constellation diagram of a 16-QAM constellation after phase noise with $\Delta\nu T_s = 6.66.10^{-6}$.

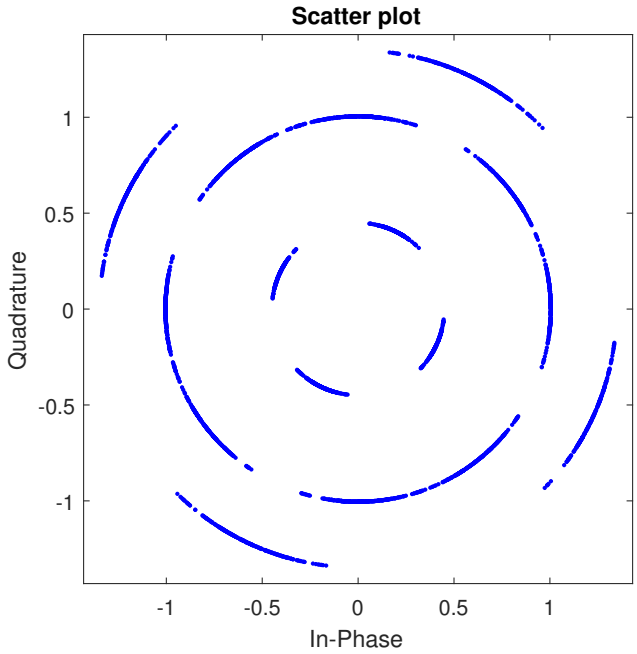

Figure 3.2 – 16-QAM constellation with phase noise.

Phase noise induces random phase shifts in the constellation, leading to symbol detection errors in phase-modulated transmissions. The phase noise reduces the signal quality and consequently increases the error rate of the communications link. To overcome these issues, the phase recovery method is an essential element in the coherent optical communication system.

3.2 Phase Recovery Algorithms

Phase recovery algorithms compensate for random phase shifts induced by the laser phase noise at both transmitter and receiver sides. There are different phase recovery algorithms that have been proposed for M-QAM modulation formats, and some are described below. Among them, the blind phase search (BPS) algorithm achieves a prominent role.

3.2.1 Viterbi and Viterbi Algorithm

The Viterbi and Viterbi algorithm is a feed-forward algorithm designed for M-PSK modulation formats. It's structure is shown in Fig. 3.3.

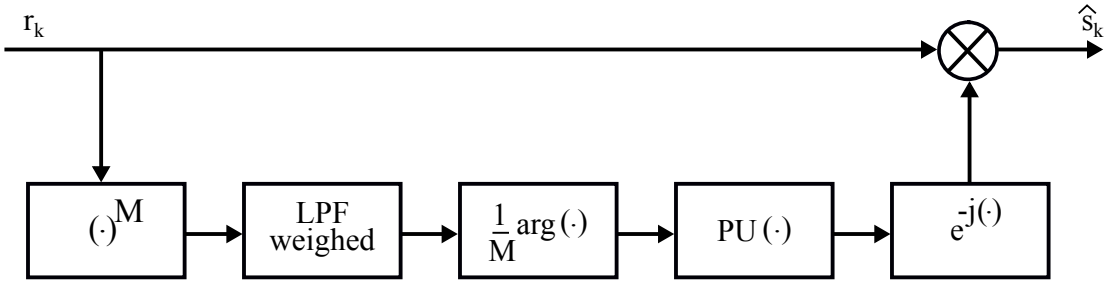

Figure 3.3 – Block diagram of the Viterbi and Viterbi algorithm.

In this algorithm, the M^{th} power of the input signal is first computed to remove the data dependency. After that, the obtained signal is subject to a filter for removing the presence of additive noise (PORTELA *et al.*, 2011), and the argument of the filtered signal is calculated and divided by M. The result is then sent to a phase unwrapper (PU) to allow an infinite phase excursion. Although the Viterbi and Viterbi algorithm is suitable for 4-QAM signals, it requires adaptations for higher-order modulation formats which impair its performance. Alternatively, decision-directed or blind-phase-search algorithms are usually deployed.

3.2.2 Decision-Directed (DD) Algorithm

The decision-directed (DD) algorithm uses previously decided symbols for removing information dependency. Fig. 3.4 shows the block diagram of the DD algorithm. The received symbol r_k is multiplied by the filtered component $e^{-j\hat{\theta}_k}$. The obtained product is sent to the decision circuit, which generates the decided symbols $\hat{s}_k$. These decided symbols are fed back and filtered to generate new estimates of $e^{-j\hat{\theta}_k}$.

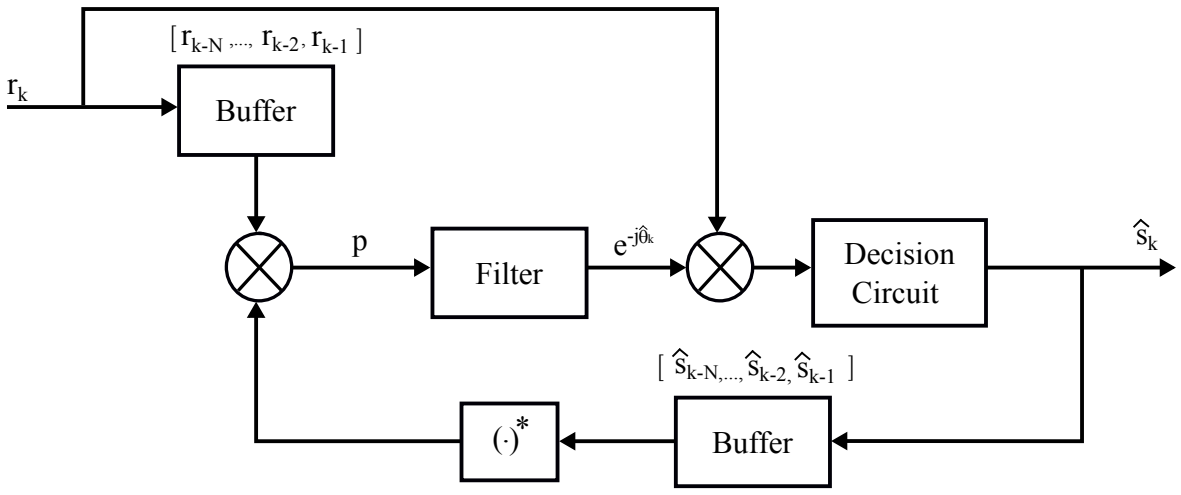

Figure 3.4 – Block diagram of a decision-directed phase recovery algorithm.

3.2.3 Blind Phase Search (BPS) Algorithm

The BPS algorithm is widely used in coherent optical systems. Fig. 3.5 shows its parallel implementation. First, the input signal r_k is sent to each of the N blocks corresponding to phase rotation n.

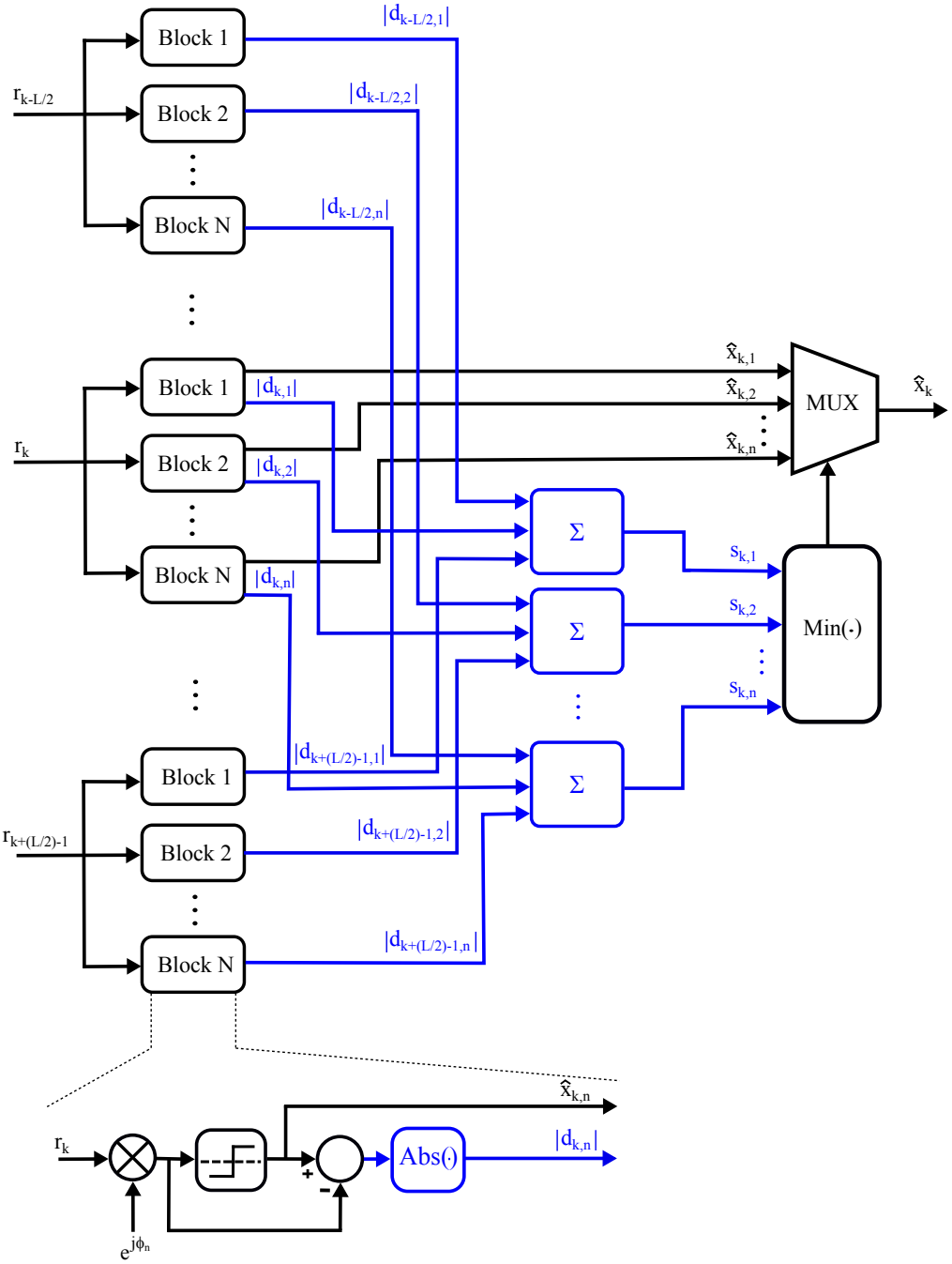

Figure 3.5 – Parallel implementation of BPS.

In each block, the given input signal is rotated by test phase angle ϕ_n:

$$\phi_n = \frac{n}{N}\frac{\pi}{2}, \quad n \in (1, 2, ..., N) \tag{3.4}$$

where N is the number of the test phase angles. After rotation, the distance $|d_{k,n}|$ to the closest constellation point $\hat{x}_{k,n}$ is calculated using:

$$|d_{k,n}| = |r_k e^{j\phi_n} - \hat{x}_{k,n}| \tag{3.5}$$

For removing noise distortions, the algorithm sums up the $|d_{k,n}|$ values of L consecutive test symbols, which are corrected with the same carrier phase angle ϕ_n, producing $s_{k,n}$. These operations require, for each symbol and test phase, L registers to store $|d_{k,n}|$ error values, and a L-sized summation block to generate $s_{k,n}$. After these operations, the optimum phase angle $\hat{x}_k$ is determined by searching the value that minimizes $s_{k,n}$.

3.3 Proposed Phase Recovery Algorithm: Forgetting Factor BPS

The BPS algorithm is widely used to recover the phase in optical signal transmissions with M-QAM formats. It is particularly attractive for having a feedforward architecture, allowing a high degree of parallelism in hardware implementations. However, in its original conception, the BPS algorithm involves filtering by a noise-rejection filter which can become extremely long when the receiver operates at high error rates, which is the case of long-haul optical systems with soft-decision FEC schemes. Alternatively, a decision-directed algorithm could circumvent this problem by recursive implementations. This solutions, however, yields a lower tolerance to phase noise and requires more complex implementation structures to enable parallelization. Alternatively, this thesis proposes a third solution which avoids long noise-rejection filters while, to some extent, preserving the BPS performance. As a drawback, the proposed solution also contains a recursive structure that requires careful implementation.

3.3.1 Forgetting Factor BPS (FF-BPS)

BPS and the proposed Forgetting Factor BPS (FF-BPS) algorithms share the general architecture shown in Fig. 3.5, but with modifications in the rotation block, as shown in Fig. 3.6. An incoming symbol r_k is fed into N equivalent blocks. Each block n is responsible for providing an estimate of the corresponding transmitted symbol $\hat{x}_{k,n}$, and an error signal $s_{k,n}$ for test phase ϕ_n. The final estimate $\hat{x}_k$ is obtained as the $\hat{x}_{k,n}$ that minimizes $s_{k,n}$. In both cases r_k is rotated by test phase ϕ_n, and a decision is made for the shortest Euclidean distance symbol $\hat{x}_{k,n}$. Signal $d_{k,n} = \hat{x}_{k,n} - r_k e^{\phi_n}$ is subsequently used to produce $s_{k,n}$.

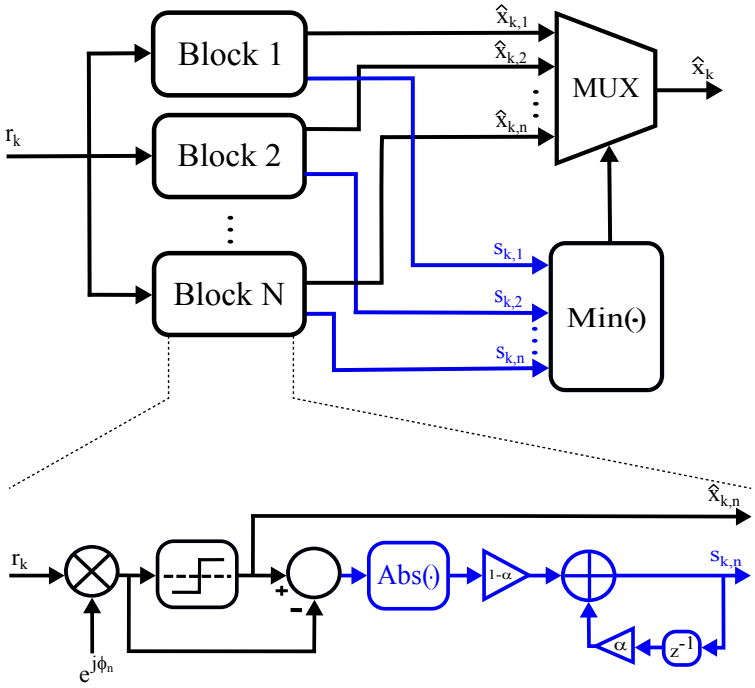

Figure 3.6 – Block diagram of Forgetting Factor BPS (FF-BPS).

The difference between both algorithms is the strategy to remove noise distortions on $s_{k,n}$. In (PFAU *et al.*, 2009), noise is filtered out by summing the error values of L consecutive test symbols that are corrected with the same carrier phase angle, where L is the size of the noise rejecting window. These operations require, for each symbol and test phase, L registers to store $|d_{k,n}|$ error values, and a L-sized summation block. In the proposed algorithm, the effects of additive noise are removed by using the forgetting factor α between error calculations. This creates a dependency between the estimated error in current and previous symbols of the form $s_{k,n} = \alpha s_{k-1,n} + (1-\alpha)|d_{k,n}|$, in which α values are typically close to 1. There are several possible architectures to implement recursive filters in pipeline for parallel processing. In one extreme, the signals would be delayed by P latches, being P the level of parallelism. In this case, long registers and adders of BPS would be replaced by latches, a multiplication by α, and a multiplication by $1-\alpha$, per sample and phase rotation. Note that the multiplication by $1-\alpha$ can be implemented at low complexity by a simple right shift, provided that $1-\alpha = 2^{-i}$, where i is integer. This also simplifies the multiplication by α, which can be implemented by a simple right shift and a subtraction, as $s_{k,n}\alpha = s_{k,n} - (1-\alpha)s_{k,n}$. On the other extreme, pipeline could be implemented without latches, but at the cost of multiplications as filter weights, noting that $s_{k+l,n} = \sum_{i=1}^{l} \left[\alpha^{l-i}(1-\alpha)|d_{k+i,n}|\right] + \alpha^l s_{k,n}$, where l=1,2,...,P. Another possible computationally-efficient method is the so-called look ahead computation (PARHI; MESSERSCHMITT, 1989). In any case, the advantages of using FF-BPS depend strongly on the ratio between L and P. It is also worth mentioning that, apart from practical hardware implementation issues, FF-BPS expressively reduces the pro-

cessing time of simulations or the post-processing of experimental data, which are usually implemented in a sequential fashion.

4 Simulation and Experimental Results

The proposed algorithm was evaluated with the 16-QAM and 64-QAM modulation formats. The 16-QAM modulation format performance was assessed using simulations and experiments, whereas the 64-QAM modulation format performance was evaluated using only simulations. The experiments were carried out but partner researchers at the CPqD research center in Campinas. The simulation and experimental setups are presented in the following sections.

4.1 Simulation Setup

At the transmit side, pseudo-random bit sequences of 2^{16} symbols are generated and mapped into a 16-QAM constellation with unitary power. The normalized input signals are rotated by Wiener phase noise corresponding to linewidths of 100 kHz at the transmitter and local oscillator lasers. The considered symbol rate for the simulation is 30 GBd. Then, AWGN is added to the rotated signal for varying the signal to noise ratio (SNR). The relation between BER and SNR for M-QAM modulation formats is theoretically represented as (PFAU *et al.*, 2009):

$$\mathrm{BER} = 1 - \left(1 - \frac{2}{\log_2(M)}\left(1 - \frac{1}{\sqrt{M}}\right) Q\left[\sqrt{\frac{3}{M-1}\mathrm{SNR}}\right]\right)^2 \tag{4.1}$$

In the simulations, SNR and OSNR are related by (ESSIAMBRE *et al.*, 2010):

$$\mathrm{SNR} = \frac{2B_{\mathrm{ref}}}{pR_s}\mathrm{OSNR} \tag{4.2}$$

where B_{ref} is the reference 12.5 GHz bandwidth, p is the number of polarization orientations and R_s is the symbol rate. At the receive side, the received signals are processed by the BPS, FF-BPS and DD algorithms using past and current symbols with 40 test phases. The simulation parameters are summarized in Table 4.2.

Table 4.1 – Simulation parameters for 16-QAM

Parameters	**Values**
Reference Bandwidth (Bref)	12.5 GHz
Symbol Rate (Rs)	30 GBd
Linewidth	100 kHz
Number of test phases (N)	40
Polarization orientations (p)	2

The performance of the DD, BPS, and the FF-BPS algorithms are also evaluated for a 64-QAM constellation through simulations. The procedures used for 16-QAM simulations are repeated for 64-QAM at the symbol rate of 30 GBaud. The considered linewidth of the transmitter and the local oscillator lasers is 100 kHz and the number of test phases used for BPS and FF-BPS is 64.

Table 4.2 – Simulation parameters for 64-QAM

Parameters	**Values**
Reference Bandwidth (Bref)	12.5 GHz
Symbol Rate (Rs)	30 GBd
Linewidth	100 kHz
Number of test phases (N)	64
Polarization orientations (p)	2

The feedforward architecture of BPS allows it to be implemented using current, future and past symbols. Conversely, because of its recursive structure, FF-BPS can only be implemented using past and current symbols. To assess the impact of this drawback, we evaluated OSNR penalty curves for BPS, DD, and FF-BPS operating with 16-QAM and 64-QAM constellations. Cycle slips associated with the phase recovery of the M-QAM signals limit the performance of the phase recovery algorithms, particularly at low OSNR regions, leading to catastrophic error sequences. Therefore, in OSNR penalty curves, cycle slips are circumvented by differential encoding and decoding. At the transmit side, differential encoding is applied to both 16-QAM and 64-QAM signals. Then the differentially encoded signals are rotated by using the Wiener phase noise. After that, the AWGN noise is added to the rotated signals.

4.2 Experimental Setup

Experimental data are also processed for the evaluation of the performance of both BPS and the FF-BPS algorithms for the 16-QAM constellation. The experimental setup is shown in Fig. 4.1. Red and black lines indicate electrical and optical signals, respectively. The addition of noise is used to simulate the combined effects of amplified spontaneous emission (ASE) and nonlinear noise after fiber propagation. At the transmit side, 2^{17} random symbols are oversampled at 2 samples per symbol and shaped using a 0.1 roll-off RC filter. The four components of the digital signal are loaded into a 64-GSa/s digital-to-analog converter (DAC) with analog 3 dB-bandwidth around 14 GHz and 8 bits of nominal vertical resolution. The electrical signals drive a dual-polarization IQ modulator (IQM) that modulates an external cavity laser (ECL) source with 100-kHz linewidth.

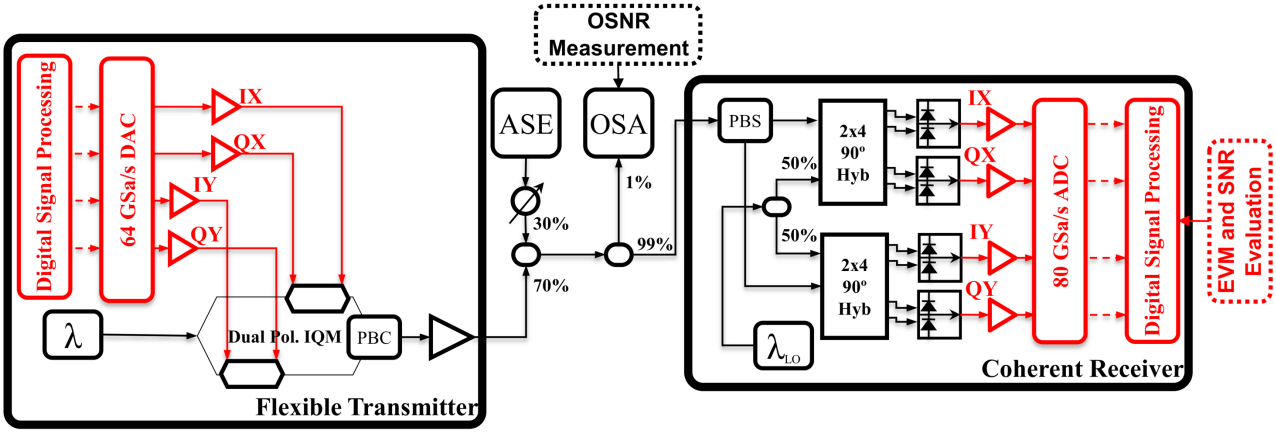

Figure 4.1 – Experimental Setup (SOUZA *et al.*, 2016).

The polarization-multiplexed (PM) optical signal is then coupled with ASE noise to vary the OSNR, which is measured through an optical spectrum analyzer (OSA). The 22-GHz polarization/phase-diversity coherent optical receiver has a free-running local oscillator (100-kHz ECL) for intradyne detection. An 80-GSa/s real-time oscilloscope (36-GHz 3 dB-bandwidth and 8 bits of nominal vertical resolution) samples the four outputs of the coherent receiver and stores the sequences for off-line processing. The sampled waveforms are equalized by conventional DSP algorithms, including (SOUZA *et al.*, 2016): (i) pre-filtering using a Matlab-designed Hamming filter with bandwidth $1.1R_s$, to match the receiver to the transmitter symbol rate; (ii) deskew (TANIMURA *et al.*, 2009) and Gram-Schmidt orthonormalization (SAVORY, 2010); (iii) clock recovery; (iv) dynamic polarization demultiplexing based on the RDE (READY; GOOCH, 1990) with 20-taps filters and $\mu = 0.001$; (v) frequency recovery using the discrete Fourier transform of the 4^{th} power of the received signal (LEVEN *et al.*, 2007);. The experimentally generated data were first recovered by using the BPS algorithm. In this case, for generating BER *versus* Window size curve, the window size is varied from 2 to 512 for different OSNR values and BER values are calculated. Then the experimental data were recovered by using the FF-BPS algorithm and the forgetting factor is varied for a set of OSNR values.

4.3 Simulation and Experimental Results

This section includes all the results obtained for 16-QAM and 64-QAM constellations by using simulations and experiments using phase recovery algorithms i.e. BPS, FF-BPS, and DD.

4.3.1 16-QAM

The simulation results for BPS and FF-BPS are shown in Fig. 4.2a and 4.2b. The horizontal dashed lines indicate the BER values without phase noise. The vertical dashed lines show the implementation-friendly forgetting factors where $1 - \alpha = 2^{-i}$, where $i = 4, 5, 7$. Clearly, both algorithms accomplished excellent phase noise tracking, exhibiting a negligible penalty. For BPS, a small L results in cycle slips, while large values impair carrier phase tracking. The optimum filter size varied from 42 at OSNR = 20 dB and BER = 10^{-3}, to 172 at OSNR = 14 dB and a BER = 6×10^{-2}. FF-BPS achieved the same minimum BER at forgetting factors varying from 0.9 to 0.999. The forgetting factor of $\alpha = 1 - 2^{-6}$ is enough to achieve penalty-free transmission with OSNRs ranging from 16 dB to 20 dB. From both figures, it is clear that the performance of the BPS simulation and FF-BPS simulation is equivalent. In the case of BPS, higher values of OSNR require low window sizes and lower values of the OSNR require high window sizes, for obtaining minimum bit error rate. Hence, for the implementation of BPS at low OSNR regions require large sized filtering windows.

The experimental results are shown in Fig. 4.2c and 4.2d. Compared with simulations, the required OSNR values are considerably higher, and the curve shapes are slightly different, as the BER exhibits floors because of the limitations in the electrical setup. The required window sizes for BPS varied from 82, for BER = 4×10^{-3} at OSNR = 34.7 dB, to 292, for BER = 7×10^{-2} at OSNR = 15 dB. FF-BPS managed to achieve an equivalent performance compared with BPS. It is interesting to observe that a forgetting factor $\alpha = 0.9922 = 1 - 2^{-7}$ achieved the minimum BER in the whole range of investigated OSNRs. Also, in the experimental case, the behavior of BPS and FF-BPS is equivalent. For BPS, the higher values of OSNR require low window size and lower values of the OSNR require high window size for obtaining minimum bit error rate.

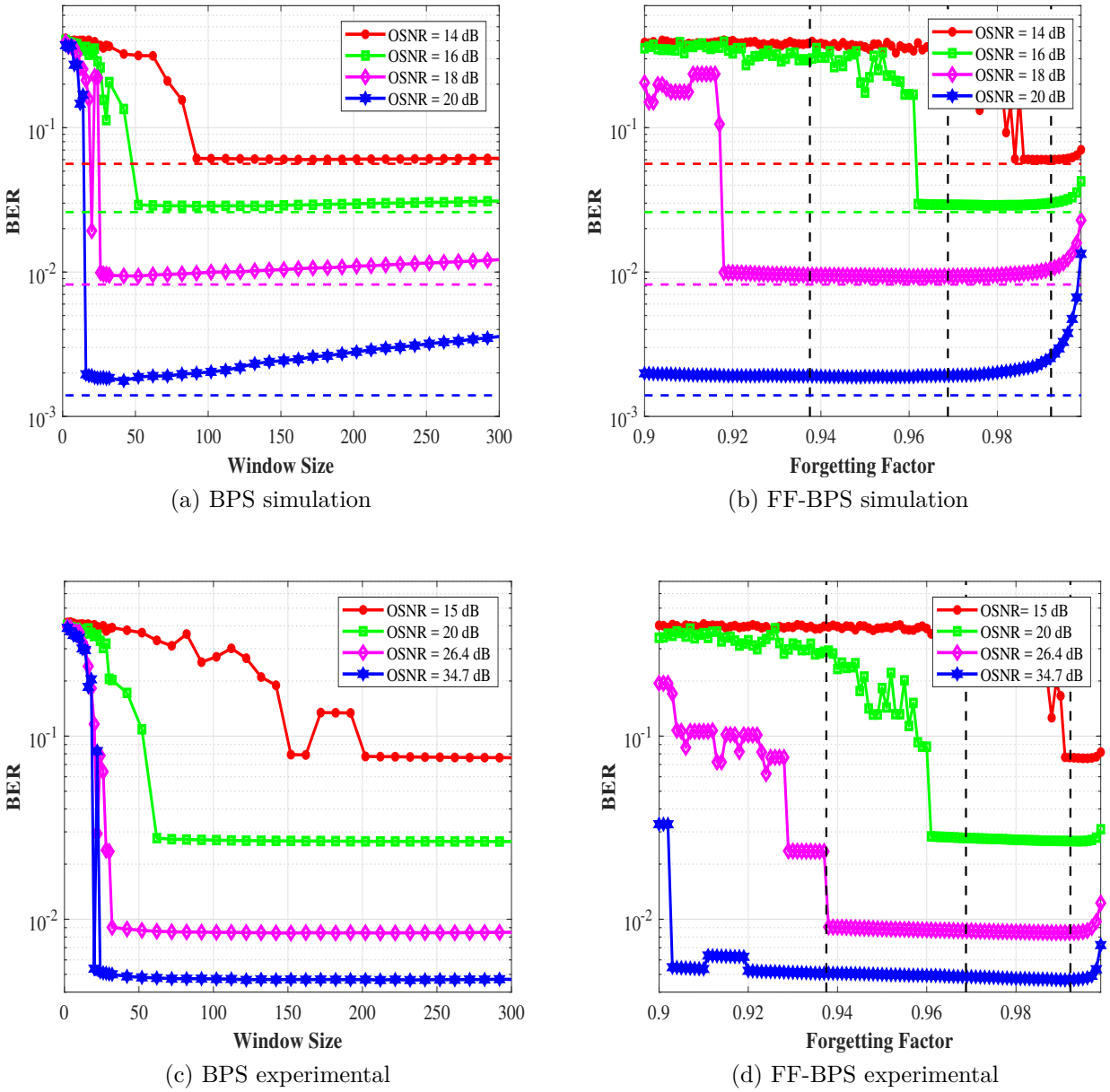

(a) BPS simulation

(b) FF-BPS simulation

(c) BPS experimental

(d) FF-BPS experimental

Figure 4.2 – BPS and FF-BPS performance in 16-QAM constellation. The vertical dotted lines indicate values suitable for hardware-efficient implementation. These simulations do not include differential decoding. Horizontal lines indicate BERs simulated without phase-noise.

The performance of the DD algorithm is also evaluated for the 16-QAM constellation through simulation. The obtained result is shown in Fig. 4.3, and the performance compared with the other two algorithms is equivalent.

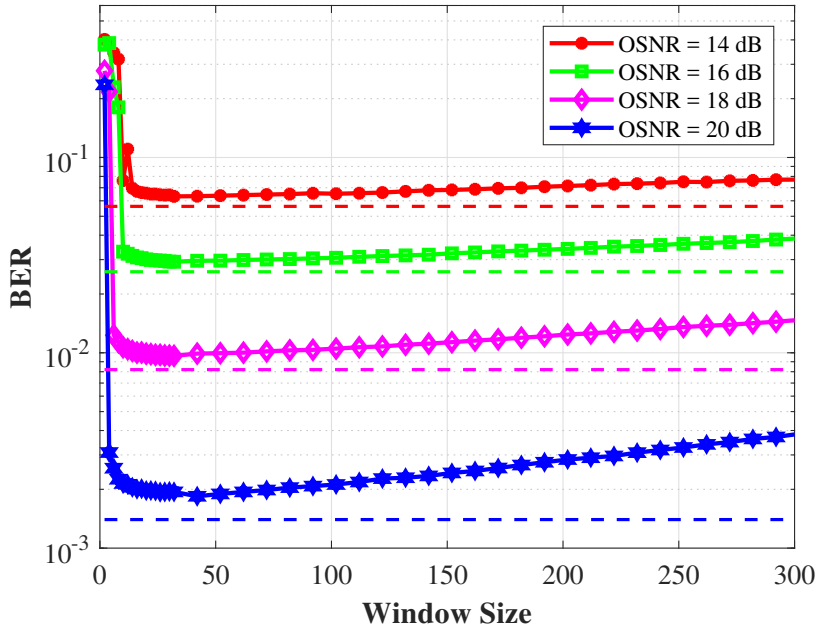

Figure 4.3 – DD performance in 16-QAM constellation. These simulations do not include differential decoding.

Fig. 4.4 shows the BER *versus* OSNR curves of BPS (current and past symbols), FF-BPS, BPS (past, current, and future symbols), and DD, respectively. The simulations have been carried out by varying the laser linewidth from 2 kHz to 6 MHz. The simulated ($\Delta\nu T_s$) products are indicated in the figures. The considered symbol rate is 30 GBd. In all the figures there exists a penalty of ≈ 0.4 dB with respect to the theoretical curve, even in the condition without laser phase noise ($\Delta\nu T_s = 0$), because of the penalty induced by the differential encoding and decoding. These results are used for obtaining OSNR penalties corresponding to different laser linewidths, as shown in Fig. 4.5.

Fig. 4.5 shows the OSNR penalty of DD, BPS (past and current symbols), FF-BPS, and BPS (past, current, and future symbols), at BER = 10^{-3}, as a function of the linewidth times symbol duration product. The OSNR penalties of the investigated algorithms are equivalent in lower values of $\Delta\nu T_s$. The DD algorithm has a high OSNR penalty compared with the proposed FF-BPS and BPS (past and current symbols). When operating with current and past samples, BPS and FF-BPS exhibit an equivalent performance and achieve a better performance compared with DD. However, BPS still outperforms the proposed FF-BPS if future samples are also used.

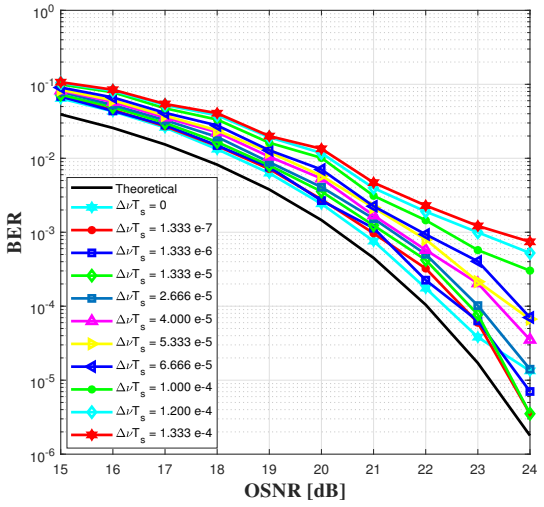

(a) BPS (current and past symbols)

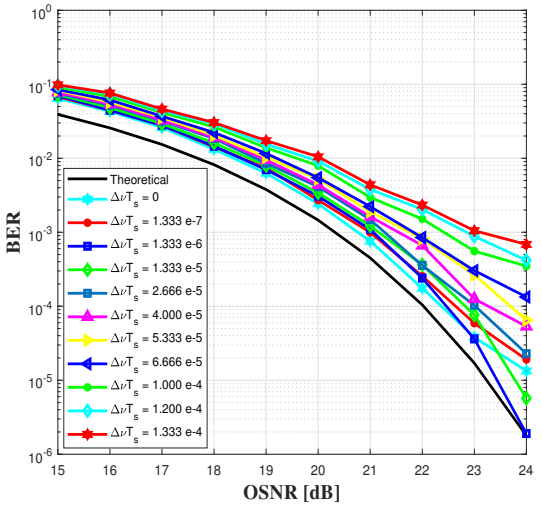

(b) FF-BPS

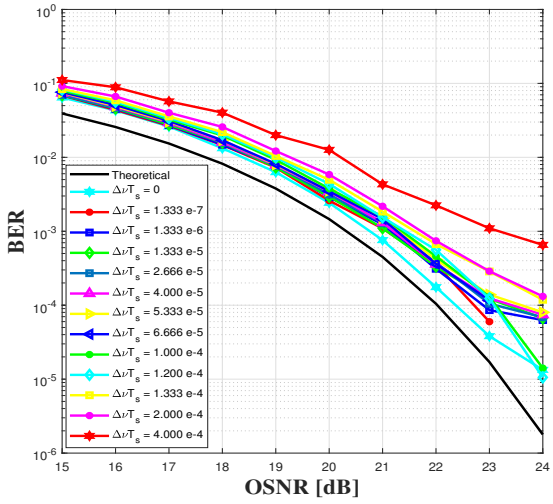

(c) BPS (past, current, and future symbols)

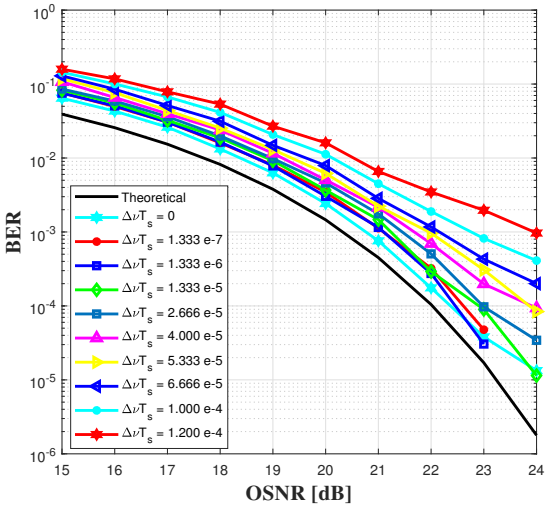

(d) DD

Figure 4.4 – BER *versus* OSNR curves for 16-QAM.

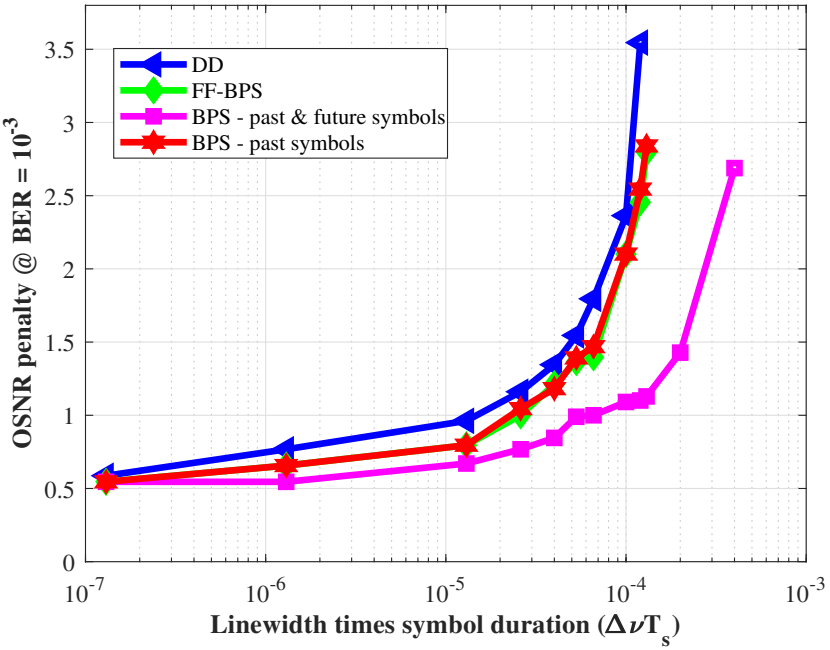

Figure 4.5 – Penalty curve for 16-QAM. These simulations include differential decoding.

4.3.2 64-QAM

The performance of the proposed FF-BPS, BPS, and DD algorithms is also evaluated in 64-QAM. The simulation results of BPS and FF-BPS are shown in Fig. 4.6a and 4.6b.

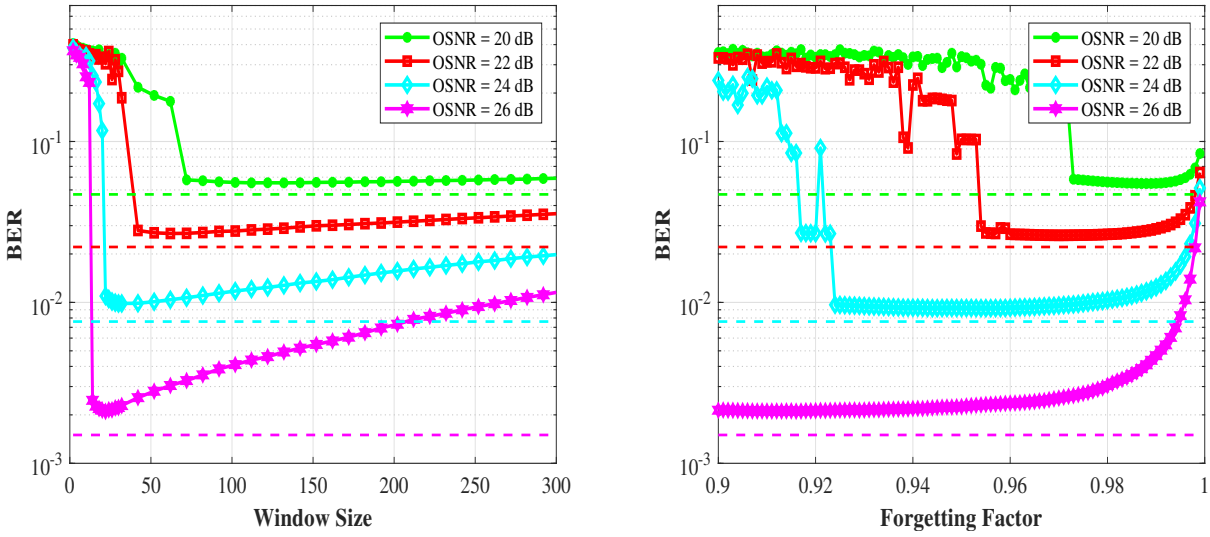

(a) BPS simulation

(b) FF-BPS simulation

Figure 4.6 – BPS and FF-BPS performance in 64-QAM constellation. Horizontal lines indicate BERs simulated without phase-noise. These simulations do not include differential decoding.

Similar to that of 16-QAM, the horizontal dashed lines indicate the BER values without phase noise. It is clear that both algorithms achieve excellent phase noise tracking with a negligible penalty. In the case of BPS, the optimum filter size varied from 22 at OSNR = 26 dB and BER = 2×10^{-3}, to 132 at OSNR = 20 dB and BER = 5×10^{-2}. FF-BPS achieved the same performance as BPS at the forgetting factors varying from 0.9 to 0.999.

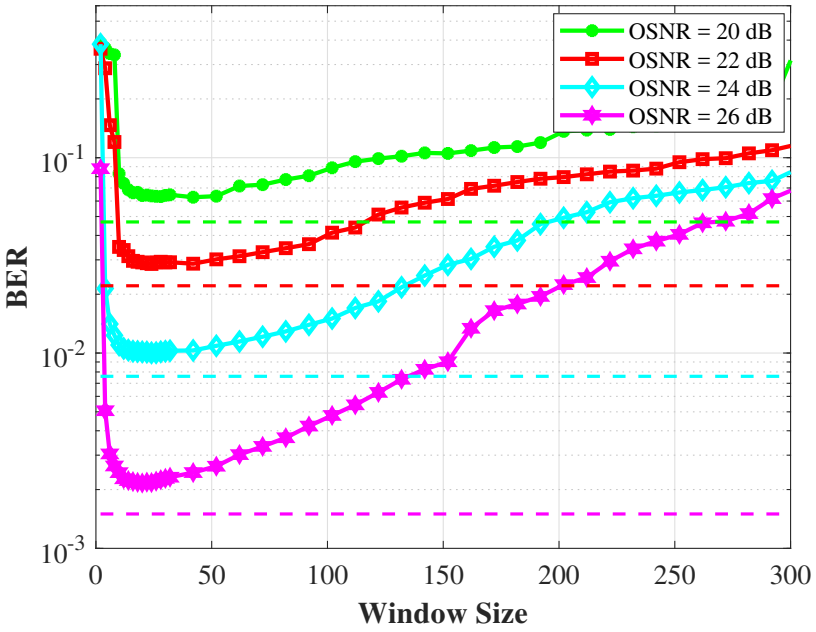

Figure 4.7 – DD performance in 64-QAM constellation. These simulations do not include differential decoding.

Fig. 4.7 shows the results obtained using the DD algorithm. Compared to FF-BPS and BPS, the DD algorithm also yields an equivalent performance when operating at the optimum window size. From the results, we can understand that the performance of the BPS (current and past symbols) algorithm and the FF-BPS algorithm is the same for 64-QAM also and the BPS (past, current, and future symbols) algorithm has better performance compared to the other two algorithms.

Fig. 4.8 indicates the BER *versus* OSNR curves of BPS (current and past symbols), FF-BPS, BPS (past, current, and future symbols), and DD for 64-QAM. For obtaining OSNR penalties corresponding to different laser linewidths, simulations have been carried out by varying the laser linewidth from 2 kHz to 1.5 MHz. There is a penalty of ≈ 0.5 dB for BER without phase noise ($\Delta\nu T_s = 0$) with respect to theory, which is the coding penalty due to differential encoding and decoding. Again, these results were used to obtain the OSNR penalties at the BER of 10^{-3}. The results of BPS (current and past symbols), FF-BPS, BPS (past, current, and future symbols), and DD are shown in Fig. 4.9. Similarly to the 16-QAM case, the OSNR penalty curves of the BPS (current and

past symbols) algorithm and the proposed FF-BPS algorithm are equivalent. The BPS (past, current, and future symbols) algorithm exhibits a superior performance compared with BPS (current and past symbols) and FF-BPS. Again, the decision directed solution exhibits the lower performance for high phase noise configurations.

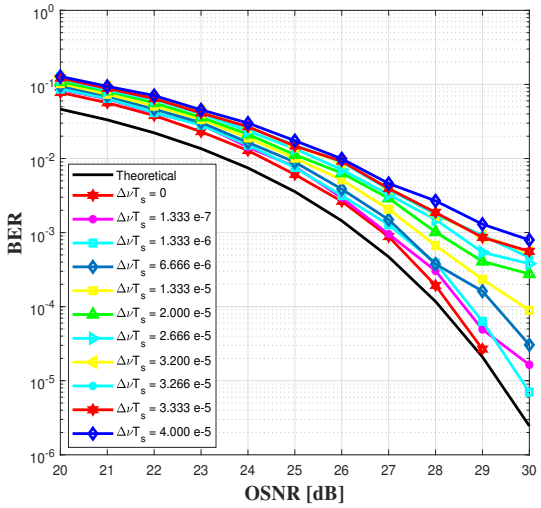

(a) BPS (current and past symbols)

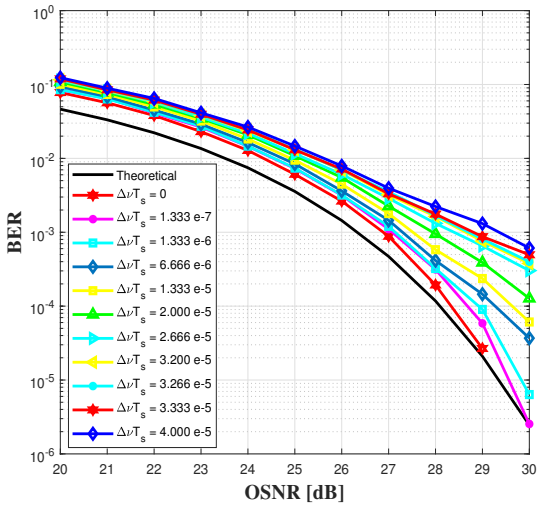

(b) FF-BPS

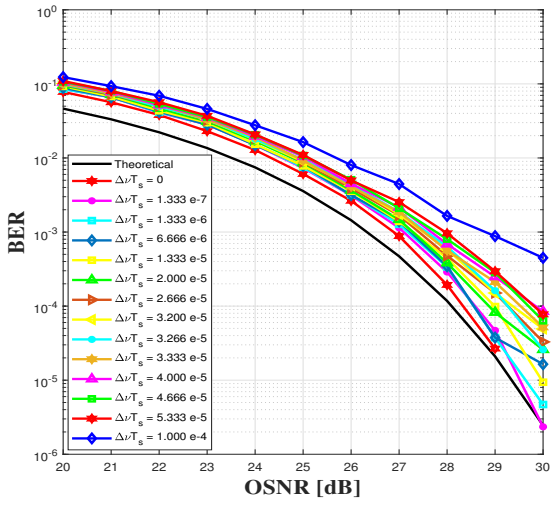

(c) BPS (past, current, and future symbols)

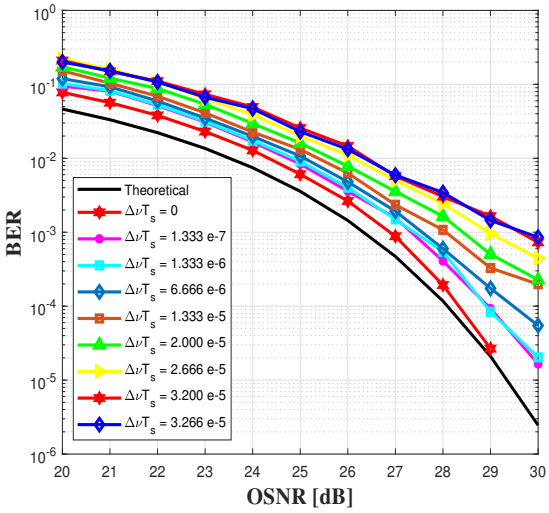

(d) DD

Figure 4.8 – BER *versus* OSNR curves for 64-QAM.

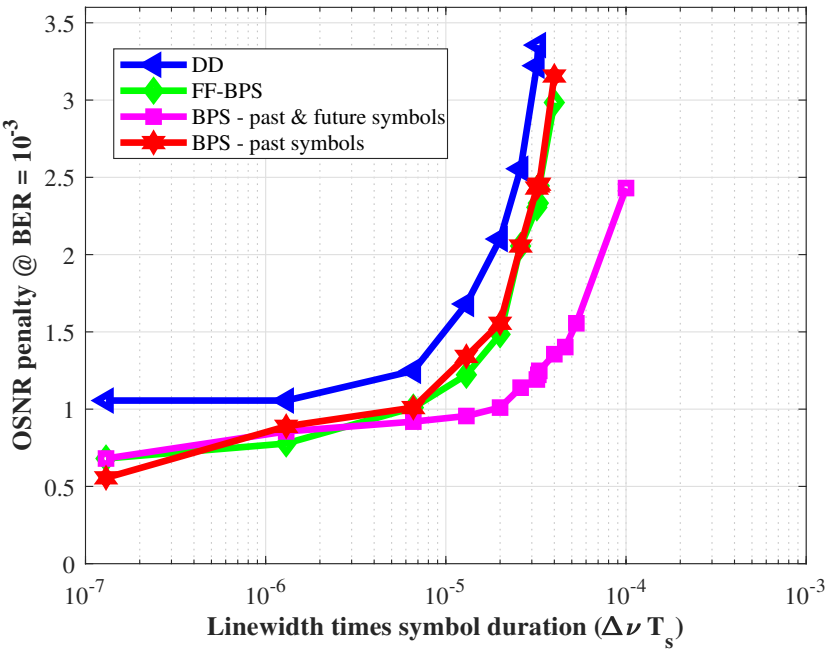

Figure 4.9 – Penalty curve for 64-QAM. These simulations include differential decoding.

In any case, for practical implementation, not all symbols in a DSP frame would have past and future neighbors. In BPS, the first symbols of the window would not have past symbols, and the last symbols of the window would not have future symbols. Therefore, although BPS would benefit from the existence of future and past symbols in the middle of the sequence, this benefit would not be extended to those in the borders of the sequence.

5 Conclusion

High-order modulation formats are an essential feature of high-speed coherent optical communication systems to increase the spectral efficiency. However, these modulation formats are less tolerant to phase noise. This leads to the requirement of phase recovery algorithms with better laser phase noise tolerance. Future optical transceivers with variable-code-rate FECs may operate at $> 10^{-2}$ error rates. In these conditions, the BPS filtering windows may require hundreds of symbols, which largely exceeds the parallelization levels desired for ASIC implementation. To circumvent this issue, we propose in this thesis a recursive BPS algorithm that replaces long filters with a forgetting factor. The proposed FF-BPS algorithm is evaluated through both simulation and experiments. The 16-QAM and 64-QAM modulation formats are investigated. The obtained results indicate equivalent performance for FF-BPS and unilateral BPS (current and past symbols) and exhibit better performance compared with DD. Bilateral BPS (past, current, and future symbols) outperforms FF-BPS and unilateral BPS. However, for practical implementations, truly bilateral BPS is usually not developed, as DSP algorithms are applied to a finite symbol sequence. Potential complexity gains of the proposed algorithm strongly depend on the implementations and the operating conditions.

Bibliography

AGRAWAL, G. P. Fiber-optic communications systems.third edition. 2002. Cited 4 times on pages 25, 26, 27, and 29.

AL-MAJMAIE, S. *IQ Imbalance Compensation: Blind versus Pilot-Based Algorithms, using Different IQ Imbalance Models*. [S.l.: s.n.], 2014. 56 p. Cited on page 31.

BARBOSA, F. A. *Avaliação da capacidade de transceptores ópticos considerando limitações de algoritmos de processamento digital de sinais*. [S.l.: s.n.], 2017. 134 p. Cited on page 36.

BORKOWSKI, R.; ZIBAR, D.; MONROY, I. T. Anatomy of a digital coherent receiver. *IEICE Transactions on Communications*, p. 1528–1536, 2014. Cited 2 times on pages 26 and 32.

CHARLET, G.; RENAUDIER, J.; MARDOYAN, H.; TRAN, P.; PARDO, O. B.; VERLUISE, F.; ACHOUCHE, M.; BOUTIN, A.; BLACHE, F.; DUPUY, J. Y.; BIGO, S. Transmission of 16.4-bit/s capacity over 2550 km using PDM QPSK modulation format and coherent receiver. *Journal of Lightwave Technology*, v. 27, n. 3, p. 153–157, Feb 2009. ISSN 0733-8724. Cited on page 18.

COELHO, L. D.; HANIK, N. Higher order modulation formats for high-speed transmission systems. In: *Proc. 1. Workshop on Optical Transmission and Equalization, 2005*. [S.l.: s.n.], 2005. p. 13–14. Cited on page 18.

DAMASK, J. *Polarization Optics in Telecommunications*. [S.l.: s.n.], 2005. Cited on page 28.

DRIS, S.; BAKOPOULOS, P.; LAZAROU, I.; SPATHARAKIS, C.; AVRAMOPOULOS, H. M-QAM carrier phase recovery using the Viterbi-Viterbi monomial-based and maximum likelihood estimators. In: *2013 Optical Fiber Communication Conference and Exposition and the National Fiber Optic Engineers Conference (OFC/NFOEC)*. [S.l.: s.n.], 2013. p. 1–3. Cited on page 18.

ESSIAMBRE, R. J.; KRAMER, G.; WINZER, P. J.; FOSCHINI, G. J.; GOEBEL, B. Capacity limits of optical fiber networks. *Journal of Lightwave Technology*, v. 28, n. 4, p. 662–701, Feb 2010. ISSN 0733-8724. Cited on page 46.

FARUK, M. S.; SAVORY, S. J. Digital signal processing for coherent transceivers employing multilevel formats. *Journal of Lightwave Technology*, v. 35, n. 5, p. 1125–1141, March 2017. ISSN 0733-8724. Cited 3 times on pages 32, 33, and 35.

FREUND, R.; NOLLE, M.; SEIMETZ, M.; HILT, J.; FISCHER, J.; LUDWIG, R.; SCHUBERT, C.; BACH, H.-G.; VELTHAUS, K.-O.; SCHELL, M. Higher-order modulation formats for spectral-efficient high-speed metro systems. In: *Optical Metro Networks and Short-Haul Systems III*. [S.l.: s.n.], 2011. v. 7959, p. 795902. Cited on page 18.

GALTAROSSA, C. R. M. A. *Polarization Mode Dispersion*. [S.l.: s.n.], 2005. 296 p. Cited 2 times on pages 9 and 28.

GAO, Y.; HA, E.; LAU, A. P. T.; LU, C.; XU, X.; LI, L. Non-data-aided and universal cycle slip detection and correction for coherent communication systems. *Opt. Express*, OSA, v. 22, n. 25, p. 31167–31179, Dec 2014. Disponível em: <http://www.opticsexpress.org/abstract.cfm?URI=oe-22-25-31167>. Cited on page 36.

GODARD, D. Self-recovering equalization and carrier tracking in two-dimensional data communication systems. *IEEE Transactions on Communications*, v. 28, n. 11, p. 1867–1875, Nov 1980. ISSN 0090-6778. Cited on page 34.

HENTSCHEL, C. *Fiber Optics Handbook: An Introduction and Reference Guide to Fiber Optic Technology and Measurement Techniques*. Hewlett-Packard, 1983. Disponível em: <https://books.google.com.br/books?id=UNJ3twAACAAJ>. Cited 2 times on pages 9 and 25.

HO, K.-P. *Phase-Modulated Optical Communication Systems*. [S.l.]: Springer US, 2005. Cited on page 29.

IP A. LAU, D. B. E.; KAHN, J. Coherent detection in optical fiber systems. v. 16, n. 2, p. 753–791, Jan 2008. Cited 2 times on pages 18 and 29.

IP, E.; KAHN, J. M. Feedforward carrier recovery for coherent optical communications. *Journal of Lightwave Technology*, v. 25, n. 9, p. 2675–2692, Sept 2007. ISSN 0733-8724. Cited on page 18.

KEISER, G. *Optical Fiber Communications*. [S.l.: s.n.], 1991. Cited 2 times on pages 9 and 27.

KIKUCHI, K. Coherent optical communications: Historical perspectives and future directions. In: NAKAZAWA; MASATAKA; KIKUCHI (Ed.). *High Spectral Density Optical Communication Technologies*. Berlin, Heidelberg: Springer Berlin Heidelberg, 2010. p. 11–49. ISBN 978-3-642-10419-0. Disponível em: <https://doi.org/10.1007/978-3-642-10419-0_2>. Cited on page 30.

KOIKE-AKINO, T.; KOJIMA, K.; MILLAR, D. S.; PARSONS, K.; MIYATA, Y.; MATSUMOTO, W.; SUGIHARA, T.; MIZUOCHI, T. Cycle slip-mitigating turbo demodulation in LDPC-coded coherent optical communications. In: *Optical Fiber Communication Conference*. Optical Society of America, 2014. p. M3A.3. Disponível em: <http://www.osapublishing.org/abstract.cfm?URI=OFC-2014-M3A.3>. Cited on page 37.

KUSCHNEROV, M.; HAUSKE, F. N.; PIYAWANNO, K.; SPINNLER, B.; ALFIAD, M. S.; NAPOLI, A.; LANKL, B. DSP for coherent single-carrier receivers. *Journal of Lightwave Technology*, v. 27, n. 16, p. 3614–3622, Aug 2009. ISSN 0733-8724. Cited on page 32.

LEVEN, A.; KANEDA, N.; KOC, U.; CHEN, Y. Frequency estimation in intradyne reception. *IEEE Photonics Technology Letters*, v. 19, n. 6, p. 366–368, March 2007. ISSN 1041-1135. Cited 2 times on pages 35 and 48.

LOUCHET, H.; KUZMIN, K.; RICHTER, A. Improved DSP algorithms for coherent 16-QAM transmission. In: *2008 34th European Conference on Optical Communication*. [S.l.: s.n.], 2008. p. 1–2. ISSN 1550-381X. Cited on page 18.

MATTHIAS; SEIMETZ. High-order modulation for optical fiber transmission. v. 143, p. 252, June 2009. ISSN 0342-4111. Cited 2 times on pages 22 and 23.

MELLO, D. A. A.; BARRETO, A. N.; LIMA, T. C. de; PORTELA, T. F.; BEYGI, L.; KAHN, J. M. Optical networking with variable-code-rate transceivers. *Journal of Lightwave Technology*, v. 32, n. 2, p. 257–266, Jan 2014. ISSN 0733-8724. Cited on page 19.

MORI, Y.; ZHANG, C.; IGARASHI, K.; KATOH, K.; KIKUCHI, K. Unrepeated 200-km transmission of 40-gbit/s 16-QAM signals using digital coherent optical receiver. In: *OECC/ACOFT 2008 - Joint Conference of the Opto-Electronics and Communications Conference and the Australian Conference on Optical Fibre Technology*. [S.l.: s.n.], 2008. p. 1–2. Cited on page 18.

NAVARRO, J.; KAKKAR, A.; SCHATZ, R.; PANG, X.; OZOLINS, O.; UDALCOVS, A.; POPOV, S.; JACOBSEN, G. Blind phase search with angular quantization noise mitigation for efficient carrier phase recovery. v. 4, p. 37, 05 2017. Cited on page 19.

NAVARRO, J. R. *Phase Noise Tolerant Modulation Formats and DSP Algorithms for Coherent Optical Systems*. [S.l.: s.n.], 2017. 67 p. Cited on page 27.

NELSON, L.; JOPSON, R. M. Introduction to polarization mode dispersion in optical systems. In: GALTAROSSA, A.; MENYUK, C. (Ed.). *Polarization Mode Dispersion*. [S.l.: s.n.], 2005. p. 1. Cited on page 28.

NOE, R. PLL-free synchronous QPSK polarization multiplex/diversity receiver concept with digital I and Q baseband processing. *IEEE Photonics Technology Letters*, v. 17, n. 4, p. 887–889, Apr 2005. ISSN 1041-1135. Cited on page 36.

PARHI, K. K.; MESSERSCHMITT, D. G. Pipeline interleaving and parallelism in recursive digital filters. i. pipelining using scattered look-ahead and decomposition. *IEEE Transactions on Acoustics, Speech, and Signal Processing*, v. 37, n. 7, p. 1099–1117, Jul 1989. ISSN 0096-3518. Cited 2 times on pages 19 and 44.

PFAU, T.; HOFFMANN, S.; NOE, R. Hardware-efficient coherent digital receiver concept with feedforward carrier recovery for M-QAM constellations. *Journal of Lightwave Technology*, v. 27, n. 8, p. 989–999, Apr 2009. ISSN 0733-8724. Cited 5 times on pages 18, 19, 39, 44, and 46.

PORTELA, T. F.; SOUTO, D. V.; ROZENTAL, V.; FERREIRA, H. B.; MELLO, D.; GRIESSER, H. Analysis of signal processing techniques for optical 112 gb/s DP-QPSK receivers with experimental data. v. 10, p. 155–164, 06 2011. Cited on page 41.

RAMASWAMI, R.; SIVARAJAN, K. *Optical Networks: A Practical Perspective*. Morgan Kaufmann Publishers, 2002. (Morgan Kaufmann series in networking). ISBN 9781558606555. Disponível em: <https://books.google.com.br/books?id=Apy17B5ZrsYC>. Cited 2 times on pages 26 and 30.

READY, M. J.; GOOCH, R. P. Blind equalization based on radius directed adaptation. In: *International Conference on Acoustics, Speech, and Signal Processing*. [S.l.: s.n.], 1990. p. 1699–1702 vol.3. ISSN 1520-6149. Cited 2 times on pages 34 and 48.

ROUDAS; IOANNIS. Coherent optical communication systems. In: ANTONIADES; (NEO), N.; ELLINAS; GEORGIOS; ROUDAS; IOANNIS (Ed.). *WDM Systems and Networks: Modeling, Simulation, Design and Engineering*. New York, NY: Springer New York, 2012. p. 373–417. ISBN 978-1-4614-1093-5. Disponível em: <https://doi.org/10.1007/978-1-4614-1093-5_10>. Cited on page 24.

ROZENTAL, V. N.; KONG, D.; FOO, B.; CORCORAN, B.; LOWERY, A. J. Cycle-slip-less low-complexity phase recovery algorithm for coherent optical receivers. *Opt. Lett.*, OSA, v. 42, n. 18, p. 3554–3557, September 2017. Disponível em: <http://ol.osa.org/abstract.cfm?URI=ol-42-18-3554>. Cited on page 19.

SALES, M.; FARUK, M. S.; SAVORY, S. J. Improved linewidth tolerant carrier phase recovery based on polar MAP metric estimate. In: *2017 Optical Fiber Communications Conference and Exhibition (OFC)*. [S.l.: s.n.], 2017. p. 1–3. Cited on page 19.

SAVORY, S. J. Digital coherent optical receivers: Algorithms and subsystems. *IEEE Journal of Selected Topics in Quantum Electronics*, v. 16, n. 5, p. 1164–1179, Sept 2010. ISSN 1077-260X. Cited 5 times on pages 18, 31, 32, 34, and 48.

SEIMETZ, M. Laser linewidth limitations for optical systems with high-order modulation employing feed forward digital carrier phase estimation. In: *OFC/NFOEC 2008 - 2008 Conference on Optical Fiber Communication/National Fiber Optic Engineers Conference*. [S.l.: s.n.], 2008. p. 1–3. Cited on page 18.

SHARIFIAN, S. *Chromatic Dispersion Compensation by Signal Predistortion:Linear and Nonlinear Filtering*. [S.l.: s.n.], 2010. 44 p. Cited 2 times on pages 27 and 33.

SOUZA, A. L. N.; RUIZ, E. J. M.; REIS, J. D.; CARVALHO, L. H. H.; OLIVEIRA, J. R. F.; ARANTES, D. S.; COSTA, M. H. M.; MELLO, D. A. A. Parameter selection in optical networks with variable-code-rate superchannels. *IEEE/OSA Journal of Optical Communications and Networking*, v. 8, n. 7, p. A152–A161, July 2016. ISSN 1943-0620. Cited 2 times on pages 9 and 48.

TANIMURA, T.; ODA, S.; TANAKA, T.; HOSHIDA, T.; TAO, Z.; RASMUSSEN, J. C. A simple digital skew compensator for coherent receiver. In: *2009 35th European Conference on Optical Communication*. [S.l.: s.n.], 2009. p. 1–2. ISSN 1550-381X. Cited 2 times on pages 31 and 48.

TARIGHAT, A.; HSU, R. C. J.; SAYED, A. H.; JALALI, B. Digital adaptive phase noise reduction in coherent optical links. *Journal of Lightwave Technology*, v. 24, n. 3, p. 1269–1276, March 2006. ISSN 0733-8724. Cited on page 18.

VITERBI, A. Nonlinear estimation of PSK-modulated carrier phase with application to burst digital transmission. *IEEE Transactions on Information Theory*, v. 29, n. 4, p. 543–551, July 1983. ISSN 0018-9448. Cited on page 18.

WU, K. T.; SUN, H. Techniques in carrier recovery for optical coherent systems. In: *OFC/NFOEC*. [S.l.: s.n.], 2012. p. 1–3. Cited on page 18.

ZHOU, X. An improved feed-forward carrier recovery algorithm for coherent receivers with M-QAM modulation format. *IEEE Photonics Technology Letters*, v. 22, n. 14, p. 1051–1053, July 2010. ISSN 1041-1135. Cited on page 18.

ZHOU, X. Efficient clock and carrier recovery algorithms for single-carrier coherent optical systems: A systematic review on challenges and recent progress. *IEEE Signal Processing Magazine*, v. 31, n. 2, p. 35–45, March 2014. ISSN 1053-5888. Cited on page 36.

ZHOU, X.; YU, J. 200-gb/s PDM-16QAM generation using a new synthesizing method. In: *2009 35th European Conference on Optical Communication*. [S.l.: s.n.], 2009. p. 1–2. ISSN 1550-381X. Cited on page 18.

ZHOU, X.; YU, J. Multi-level, multi-dimensional coding for high-speed and high-spectral-efficiency optical transmission. *Journal of Lightwave Technology*, v. 27, n. 16, p. 3641–3653, Aug 2009. ISSN 0733-8724. Cited on page 18.

ZHUGE, Q.; CHEN, C.; PLANT, D. V. Low computation complexity two-stage feedforward carrier recovery algorithm for M-QAM. In: *2011 Optical Fiber Communication Conference and Exposition and the National Fiber Optic Engineers Conference*. [S.l.: s.n.], 2011. p. 1–3. Cited on page 19.